RSC Medicinal Chemistry

ROYAL SOCIETY OF CHEMISTRY

RESEARCH ARTICLE

View Article Online
View Journal

Cite this: DOI: 10.1039/d6md00312e

Design, synthesis, and X-ray structural studies of potent SARS-CoV-2 Mpro inhibitors containing tetrahydroisoquinoline-3-carboxamides as P2 ligands

Arun K. Ghosh, *[ab] Ashish Sharma,[a] Satyanarayana Iddum,[a] Sydney N. Bogan, [c] Uttara Jayashankar, [d] Emma K. Lendy,[c] Shin-ichiro Hattori, [e] Nobuyo Higashi-Kuwata, [e] Hiroaki Mitsuya [efg] and Andrew D. Mesecar [acd]

Received 20th April 2026,
Accepted 9th June 2026

DOI: 10.1039/d6md00312e

rsc.li/medchem

Structure based design, synthesis and evaluation of a series of potent SARS-CoV-2 main protease inhibitors are described. We designed conformationally constrained tetrahydroisoquinoline-3-carboxamides as P2 ligands. The studies involved structure–activity relationship studies by varying P1, P2, P3, and P4 ligands, including five- and six-membered lactam rings as P1 ligands as well as nitrile and thiazole heterocycles as P1′ ligands. These new inhibitors exhibited potent SARS-CoV-2 Mpro inhibitory activity. Several inhibitors also blocked the replication of SARS-CoV-2 in VeroE6 cells with low nanomolar EC_{50} values, more potent than the approved drug, nirmatrelvir. Inhibitor **5j** displayed an Mpro inhibitory K_i of 1.2 nM and antiviral EC_{50} value of 360 nM. We determined several high-resolution X-ray structures of inhibitor-SARS-CoV-2 Mpro complexes which provided important insights into the ligand-binding site interactions in the active site.

Introduction

The COVID-19 pandemic is considered the most consequential global health crisis since the 1918 influenza pandemic.[1,2] The pandemic caused by SARS-CoV-2 lasted over three years and imposed serious uncertainties around the world. The World Health Organization reported over 778 million confirmed cases and more than 7 million deaths as of late 2023.[3,4] The actual death toll is likely to be much higher due to inconsistent testing, reporting, and data collection during that time. The development of COVID-19 vaccines played a pivotal role in the fight against this outbreak.[5,6] However, the lack of herd immunity and the occurrence of other new variants represented major challenges of vaccination.[7,8] Since the outbreak, drug development efforts towards effective treatment of COVID-19 have also been pursued rapidly.[9–11] Molecular events critical to SARS-CoV-2 replication provided a number of important biochemical targets for drug development. At the first stage of infection, SARS-CoV-2 binds to the host cell surface receptor angiotensin converting enzyme 2 (ACE2) to enter the cell. Following cell entry, viral RNA attaches to the host cell ribosome to produce two polyproteins, pp1a and pp1ab. These proteins are then cleaved by the coronavirus main protease (Mpro) and papain-like protease (PLpro).[12–14] Subsequent cleavage of these polyproteins results in the formation of several other critical enzymes including RNA-dependent RNA polymerase (RdRp) for genome replication.[15] Many of these key enzymes were intensively targeted for SARS-CoV antiviral drug development.[9–11]

Early on, SARS-CoV-1 main protease (Mpro) was recognized as one of the most promising targets because of its essential role in viral replication and transcription of viral genome.[16,17] During the SARS-CoV-1 outbreak in 2002, this homomeric enzyme was recognized as an excellent target for antiviral drug development. SARS-CoV Mpro contains a Cys-His catalytic dyad in the active site.[18,19] The nucleophilic Cys145 in the active site was then identified as a key residue to target for drug design.[20–22] Past and present research efforts targeting this Mpro led to the development

[a] Department of Chemistry, Purdue University, 560 Oval Drive, West Lafayette, IN 47907, USA. E-mail: akghosh@purdue.edu
[b] Department of Medicinal Chemistry and Molecular Pharmacology, Purdue University, West Lafayette, IN 47907, USA
[c] Department of Biochemistry, Purdue University, West Lafayette, IN 47907, USA
[d] Department of Biological Sciences, Purdue University, West Lafayette, IN 47907, USA
[e] Department of Refractory Viral Diseases, National Center for Global Health and Medicine, Shinjuku, Tokyo 162-8655, Japan
[f] Department of Infectious Diseases, Kumamoto University School of Medicine, Kumamoto 860-8556, Japan
[g] Experimental Retrovirology Section, HIV and AIDS Malignancy Branch National Cancer Institute, Bethesda, MD 20892, USA

of covalent inhibitors with electrophilic warheads like α,β-unsaturated esters, α-ketoamides, aldehydes, and α-ketobenzothiazoles.[9,23,24] Representative inhibitors, **1** with an α,β-unsaturated ester warhead and α-ketobenzothiazole **2** (Fig. 1), were demonstrated to both inhibit SARS-CoV-1 Mpro and SARS-CoV-2 Mpro.[25–27] The X-ray structural studies with inhibitor-bound Mpro showed the formation of a covalent bond with Cys145 in the Mpro active site. The majority of early research efforts targeting SARS-CoV-1 Mpro led to the development of covalent inhibitors with electrophilic warheads like α,β-unsaturated esters, α-ketoamides, aldehydes, and α-ketobenzothiazoles as represented in compounds **1** and **2**.[23–27] Subsequent development of SARS-CoV-2 Mpro inhibitors led to potent peptidomimetic and non-peptide Mpro inhibitors with therapeutic potential for treatment of COVID-19.[9–11,23,24]

Nirmatrelvir (**3**) became the first orally active Mpro inhibitor drug for the treatment of COVID-19.[28,29] The key structural features of nirmatrelvir include a P1′ nitrile, a P1 5-membered lactam, P3–P4 *tert*-butyl trifluoro acetamide, and a *gem*-dimethyl cyclopropyl proline derivative inherent to boceprevir (**4**).[30,31] Nirmatrelvir was approved as a combination therapy named Paxlovid® that is co-formulated with ritonavir, a CYP3A4 inhibitor, to boost pharmacokinetic properties.[32,33] Paxlovid® has become the mainstream drug choice for treatment of SARS-CoV-2 infection and COVID-19.[34,35] However, Paxlovid® treatment is not ideal as it exhibits considerable side effects, including drug–drug interactions and viral rebound-effects.[36,37] To date several other SARS-CoV-2 Mpro inhibitor drugs have been in active clinical trials for treatment of COVID patients and for long COVID syndrome.[11,38,39] As part of our continuing interest in the development of novel SARS-CoV-2 Mpro inhibitors, we used structure-based design approaches and investigated a new class of conformationally constrained P2-scaffolds in combination with P1′ electrophilic warheads such as nitriles and ketothiazole functionalities that can form covalent bonds with catalytic Cys145 in the active site. Herein, we report the results of our studies which demonstrate that the stereochemically defined (*S*)-tetrahydroisoquinoline (THIQ)-3-carboxamide derivatives can be well accommodated by the S2- subsite of the SARS-CoV-2 Mpro active site. Several derivatives incorporating these heterocyclic templates exhibited very potent SARS-CoV-2 Mpro inhibitory activity as well as potent low nanomolar antiviral activity comparable to nirmatrelvir and other clinical inhibitors. We have determined the high resolution X-ray crystal structure of inhibitor-bound SARS-CoV-2 Mpro which shows critical ligand-binding site interactions responsible for potent inhibitory activity.

Results and discussion

The X-ray structure of nirmatrelvir-bound SARS-CoV-2 Mpro highlights important interactions between nirmatrelvir and the Mpro active site.[28,40] As highlighted in Fig. 2, the

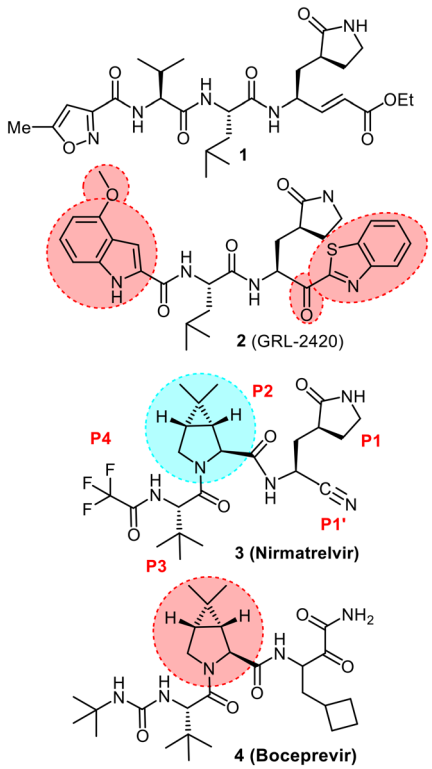

Fig. 1 Structure of nirmatrelvir **3**, showing P1–P4 moieties, and structures of compounds **2**–**4**.

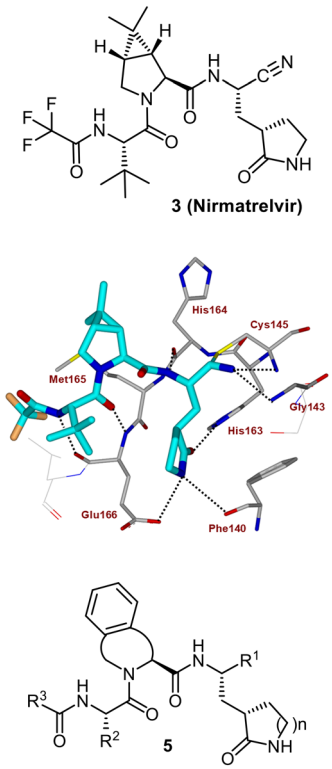

Fig. 2 Design strategy for tetrahydroisoquinoline-3-carboxamide-derived inhibitors.

warhead P1′-nitrile functionality formed a covalent bond with the catalytic Cys145 and made a thioimidate adduct in the S1 and S1′ subsites. The P1 lactam carbonyl oxygen formed a hydrogen bond with His163, and the lactam NH formed a strong hydrogen bond with the Glu166 side chain carboxylic acid in the S1 subsite. The P2 bicyclic proline moiety occupied the hydrophobic pocket surrounding His41, Met49, Tyr165, Arg188 and Gln189. The other key interaction involved the formation of a pair of hydrogen bonds through the P3-amide carboxy oxygen and the backbone Glu166 amide as well as through the P4-trifluoroacetamide carboxy oxygen and the Glu166 side chain in the S4 subsite. The P3-*tert*-butyl group is mostly solvent exposed and appears to accommodate a slightly larger hydrophobic moiety. Based upon these structural insights, we hypothesized that a slightly more sterically demanding bicyclic THIQ ring with appropriate stereochemistry on the carboxamide functionality can be suitably accommodated by the S2 subsite binding pocket and *tert*-butyl group at the P3 position. We presumed that the lipophilic THIQ heterocycle may further improve antiviral activity and overall drug properties. Such structural features are imbedded in numerous bioactive molecules and approved drugs.[41,42] We also designed different combinations of the adjacent P3-hydrophobic group with electrophilic warheads such as nitrile and ketobenzothiazole moieties to optimize favorable van der Waals contacts and warhead reactions with Cys145.

Our synthetic strategy for the preparation of various SARS-CoV-2 Mpro inhibitors incorporating the THIQ scaffold as the P2 ligand along with diverse P1′, P1, P3, and P4 modifications is outlined in Scheme 1. Our plan was to conduct modular variation at these key positions through the coupling of carboxylic acids derived from methyl esters of dipeptide intermediates **6** with various amine warheads **7**, obtained from five- and six-membered lactam precursors. Carboxylic acid segment **8** was prepared by amide coupling of readily available amino acids, optically active tetrahydroisoquinoline derivatives that are commercially available. This modular approach was designed to rapidly assemble a selected group of SARS-CoV-2 Mpro inhibitors with systematic variations of the other ligands to probe structure–activity relationships.

The synthesis of the target amine intermediates **7** is shown in Scheme 2. Lactam derivatives **7a** and **7b** were synthesized according to our recently developed protocol.[22,43] Treatment of **10a** and **10b** with ammonium hydroxide in methanol at 23 °C for 12 h afforded the corresponding carboxamide derivatives. Subsequent reaction of the carboxamides with *p*-toluenesulfonyl chloride (TsCl) and pyridine furnished the nitrile derivatives **7a** and **7b** in overall yields of 58% and 56%, respectively, over two steps.[42,43] The synthesis of benzothiazole and 4-phenylthiazol ketone warheads began with base-mediated ester hydrolysis of **10a** and **10b** using LiOH to yield the corresponding carboxylic acids. Activation of the acids with EDCI and HOBt, followed by coupling with *N*,*O*-dimethyl hydroxylamine hydrochloride in the presence of triethylamine, afforded the Weinreb amides **11a** and **11b** in 85% and 84% overall yields over two steps.[26,27] Subsequent addition of lithiated benzothiazole or 4-phenylthiazole nucleophiles to **11a** and **11b** in anhydrous THF at −78 °C provided the corresponding ketone derivatives **12a**, **12b**, **13a**, and **13b** in good yields as shown in Scheme 2.

The synthetic route for the preparation of various modified P2, P3, and P4 dipeptide carboxylic acid derivatives is illustrated in Scheme 3. Our synthetic strategy involved coupling of commercially available (*S*)-methyl 1,2,3,4-

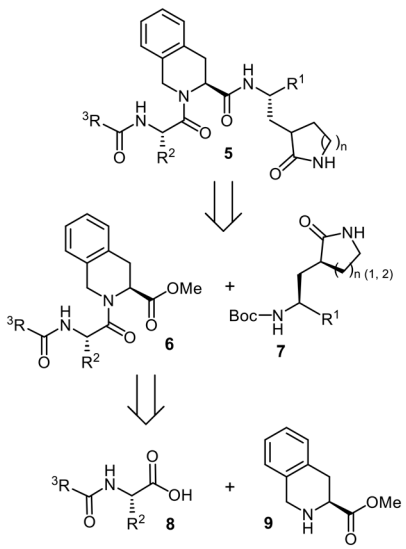

Scheme 1 Synthetic strategy for inhibitors **5**.

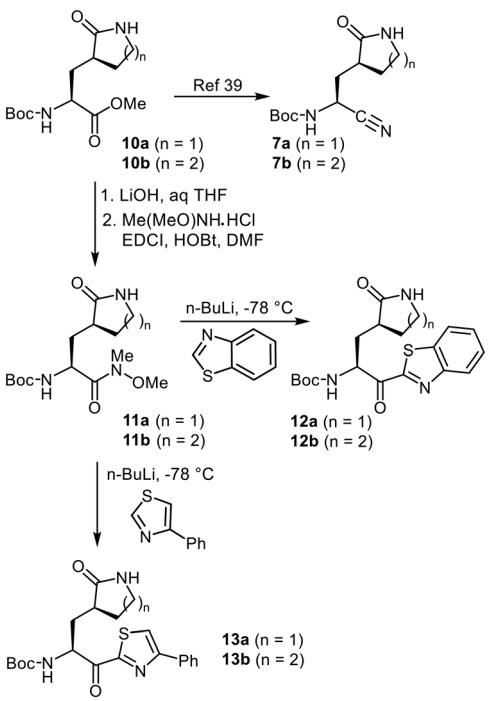

Scheme 2 Asymmetric synthesis of various amines.

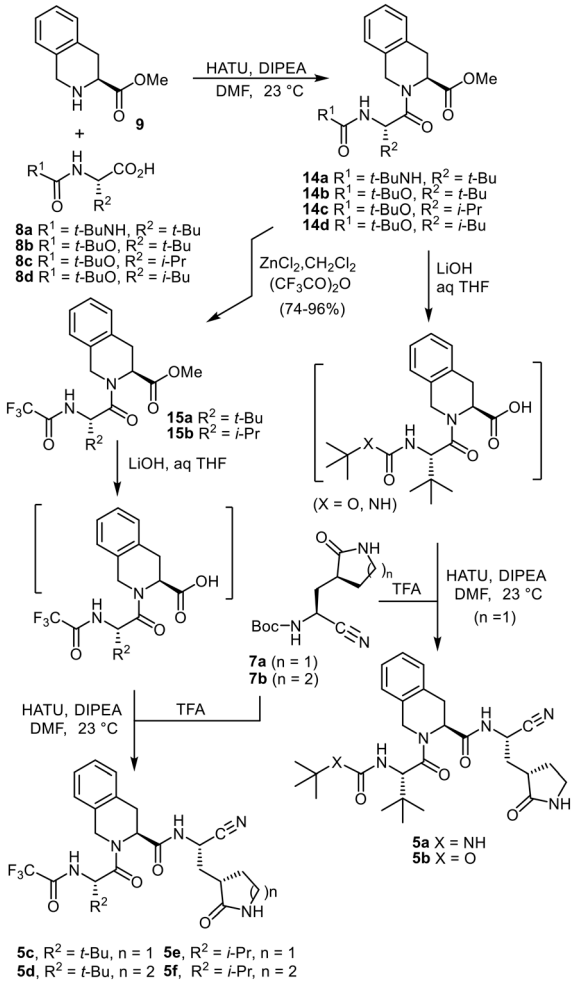

Scheme 3 Synthesis of protease inhibitors **5a**–**5d**.

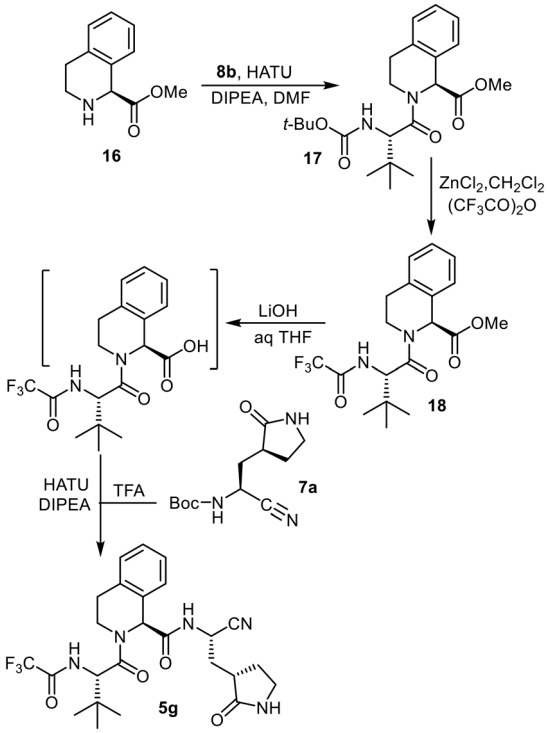

Scheme 4 Synthesis of protease inhibitor **5g**.

tetrahydroisoquinoline-3-carboxylate hydrochloride amine **9** with *N*-*tert*-butylformamide-L-*tert*-leucine (**8a**), *N*-Boc-L-*tert*-leucine (**8b**), *N*-Boc-L-valine (**8c**), and *N*-Boc-L-leucine (**8d**), using HATU as a coupling reagent and DIPEA as a base to afford the corresponding dipeptide esters **14a–14d** in excellent yields. Introduction of a trifluoroacetamide moiety as a P4 modification was carried out using our previously described protocol to reduce racemization.[43,44] Treatment of dipeptide esters **14b** and **14c** with 10% anhydrous $ZnCl_2$ in CH_2Cl_2 followed by trifluoroacetic anhydride (TFAA) at room temperature for 12 h afforded the corresponding trifluoroacetamide derivatives **15a** and **15b** in 81%, and 76% yields, respectively. Dipeptide derivatives **14a**, **14b** and trifluoroacetamide derivatives **15a**, **15b** were converted to nitrile derivatives **5a**, **5b**, **5c**, and **5e** using a two-step sequence involving saponification of esters **14a**, **14b**, **15a**, **15b** followed by coupling of the resulting acids with amine derived from **7a** after removal of the Boc-group with trifluoroacetic acid. Similarly, trifluoroacetamide derivatives **15a**, **15b** were converted to nitrile derivatives **5d**, and **5e** by coupling of the resulting acids with amine derived from **7b** after removal of the Boc-group as shown.

We incorporated a regioisomeric replacement of amine **9** as shown in Scheme 4. Commercially available (*S*)-methyl 1,2,3,4-tetrahydroisoquinoline-1-carboxylate hydrochloride amine **16** was coupled with *N*-Boc-L-*tert*-leucine **8b** to afford dipeptide **17** in 77% yield. It was converted to trifluoroacetamide derivative **18** using our previous protocol.[43,44] The trifluoroacetamide derivative **18** was then transformed into compound **5g** using a two-step sequence involving saponification of ester **18** followed by coupling of the resulting acid with the amine derived from **7a** to provide **5g** in 42% yield.

Synthesis of derivatives containing five- and six-membered lactam P1-ligands and benzothiazoles as electrophilic warheads is shown in Scheme 5. Saponification of ester in dipeptide derivatives **14b**, **15a**, and **18** yielded the corresponding carboxylic acids, which were subjected to amide bond formation *via* coupling with amines derived from **12a** and **12b** following Boc-group deprotection, to afford the target protease inhibitors **5h–5k**. Synthesis of derivatives bearing 4-phenylthiazole as the warhead is shown in Scheme 6. Treatment of Boc-protected amines **13a** and **13b** with trifluoroacetic acid (TFA) in dichloromethane at 23 °C removed the Boc group to furnish the corresponding free amines. The resulting amines were coupled with carboxylic acids derived from dipeptides **14b** and **15a** using standard peptide coupling conditions and afforded the target inhibitors **5l–5n** in good to excellent yields.

We recently reported GRL-2420 containing a 4-methoxy-indole carboxamide P4 ligand as a potent SARS-CoV-2 Mpro inhibitor.[27] To further optimize ligand combination with the

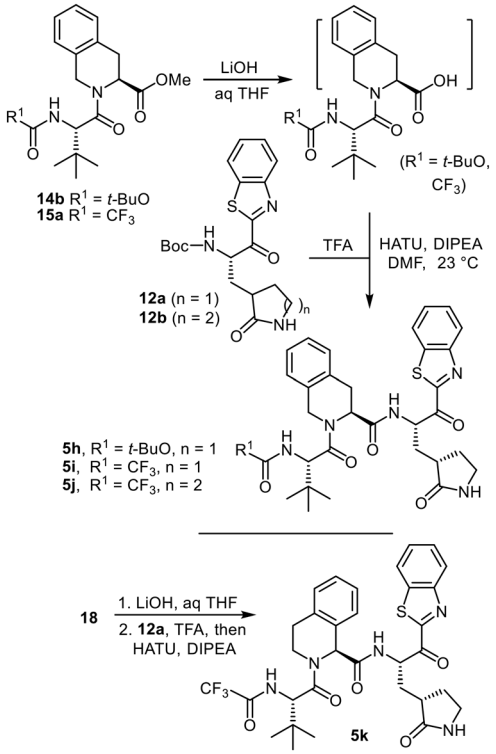

Scheme 5 Synthesis of protease inhibitors **5h–k**.

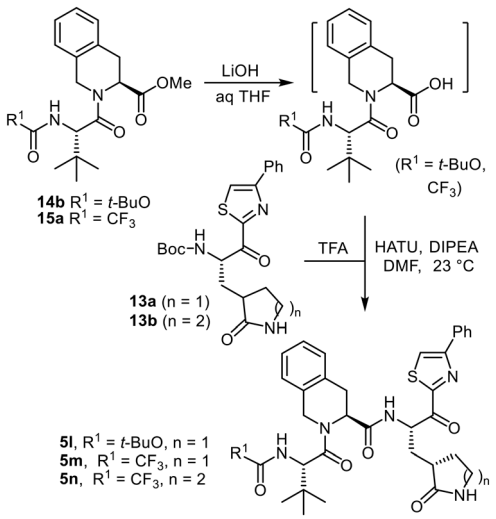

Scheme 6 Synthesis of protease inhibitors **5l–n**.

THIQ scaffold, we examined leucine and 4-methoxyindole-2-carboxylic acid modifications at the P3 and P4 positions. Synthesis of derivatives **5o–p** is shown in Scheme 7. Compound **14d** was subjected to Boc deprotection with TFA and coupling of the resulting amine with acid **19** using HATU and DIPEA, which afforded compound **20** in 62% overall yield. Hydrolysis of the ester in **20** yielded the corresponding carboxylic acid. The resulting acids were coupled with amines derived from **7b**, **13a**, and **13b** after Boc removal, to furnish inhibitors **5o–5q** in good yields.

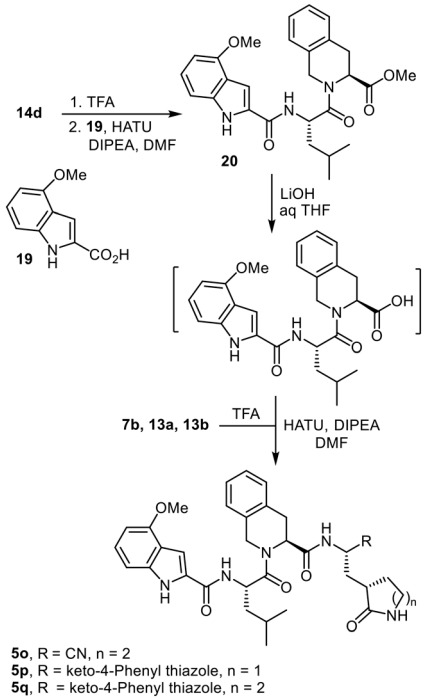

Scheme 7 Synthesis of Mpro inhibitors **5o–q**.

The main design goal for these inhibitors containing conformationally constrained THIQ ligands was to promote enhanced interactions in the active site specifically within the S2 pocket. In particular, we planned to modulate van der Waals and hydrogen bonding interactions with other ligand combinations to improve *in vitro* activity and drug properties. The structure and *in vitro* activity of synthetic compounds are shown in Table 1. Our previously reported assay protocols were utilized for evaluation of SARS- CoV-2 Mpro inhibitory activity as well as antiviral activity in VeroE6 cells.[27,45] Our in-house prepared nirmatrelvir compound showed potent SARS-CoV-2 Mpro inhibition activity with a K_i value of 0.26 nM and antiviral EC_{50} value of 2 μM. In compound **5a**, we incorporated a P2 (*S*)-tetrahydro-isoquinoline-3-carboxamide and a P4 *tert*-butyl urea functionality which is inherent to boceprevir **3**.[26,27] These changes resulted in compound **5a** which showed over 70-fold loss of both Mpro inhibitory activity compared to nirmatrelvir. Compound **5a** did not exhibit any appreciable antiviral activity (entry 2). Incorporation of a similar sterically demanding Boc group resulted in compound **5b** which showed further loss of Mpro inhibitory activity. Compound **5b** exhibited an antiviral EC_{50} value of 34.2 μM (entry 3). The effect of the trifluoroacetamide P4 ligand of nirmatrelvir was examined in compound **5c** which showed improvement of Mpro inhibitory activity, but no change of antiviral activity compared to **5b** (entries 3 and 4). We then examined the effect of the 6-membered lactam in combination with the P2-tetrahydroisoquinoline group in compound **5d**. As can be seen, the 6-membered lactam resulted in 2-fold improvement of Mpro inhibitory activity and nearly 16-fold

Table 1 SARS-CoV-2 3CLpro inhibition by nirmatrelvir derivatives **5a–q**

Entry	Inhibitor	K_i or IC_{50}[a] (nM)	EC_{50}[b] (μM)
1	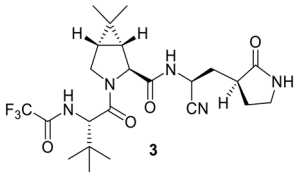 **3**	0.26	2.0
2.	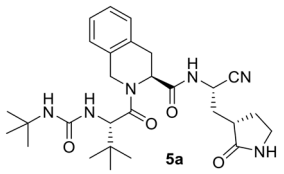 **5a**	18.7	>100
3	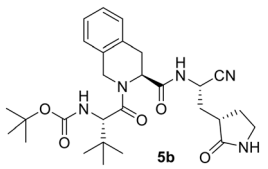 **5b**	50.4	34.2
4	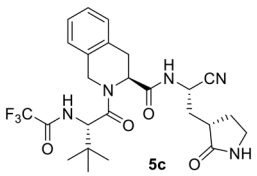 **5c**	6.4	35.5
5	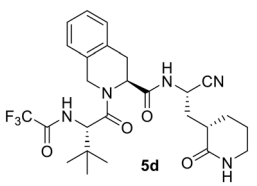 **5d**	3.2	2.2
6	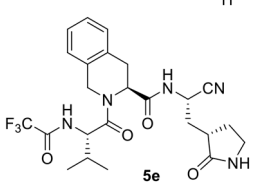 **5e**	270	40.5
7	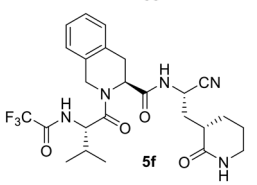 **5f**	172.8	44.5
8.	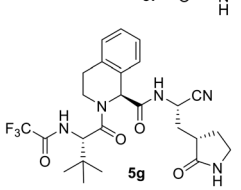 **5g**	276.1	28.3
9.	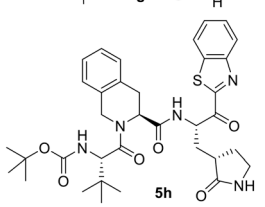 **5h**	171.4	0.8

Table 1 *(continued)*

Entry	Inhibitor	K_i or IC_{50}[a] (nM)	EC_{50}[b] (μM)
10.	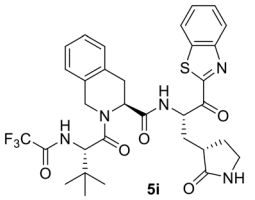 5i	75	1.1
11.	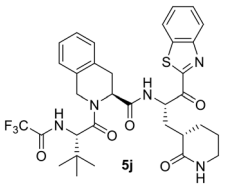 5j	1.2	0.36
12.	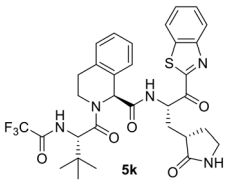 5k	123	3
13.	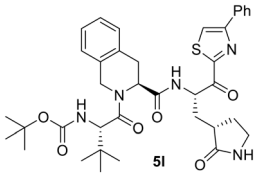 5l	112	1.9
14.	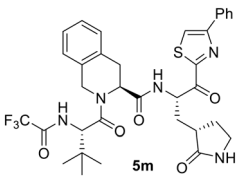 5m	2.0	2.7
15.	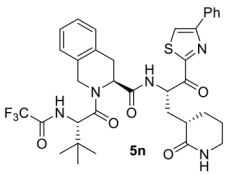 5n	51.6	2.6
16.	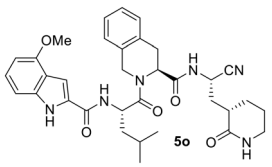 5o	189.4	23.5
17.	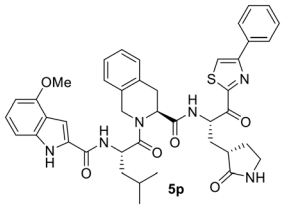 5p	310	nd[c]

Table 1 *(continued)*

Entry	Inhibitor	K_i or IC_{50}[a] (nM)	EC_{50}[b] (μM)
18.	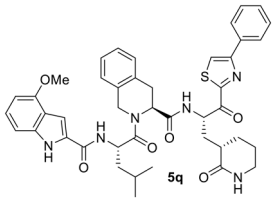 **5q**	400	nd[c]

[a] K_i values were determined from fitting inhibition data to the Morrison equation as described.[43] [b] EC_{50} values are means of at least four experiments. [c] nd, not determined.

improvement of antiviral activity (entry 5). This result is consistent with our previous observation, where 6-membered lactam in nirmatrelvir improved *in vitro* activity significantly.[44]

We then investigated a slightly less sterically demanding isopropyl side chain in place of the P3-*tert*-butyl group in combination with 5- and 6-membered lactams. The resulting compounds **5e** and **5f** with the P2 tetrahydroisoquinoline scaffold showed significant loss of *in vitro* activity (entries 6 and 7). We also investigated the effect of isomeric tetrahydroisoquinoline-2-carboxamide in compound **5g**, which exhibited over 40-fold loss of Mpro inhibitory activity compared to compound **5c**, indicating that the tetrahydroisoquinoline-3-carboxamide moiety is preferred by the S2 subsite. In compound **5h**, we examine the effect of keto-benzothiazole in place of the nitrile P1′-group. Interestingly, these changes resulted in nearly 3-fold loss of Mpro inhibitory activity compared to compound **5b** with a P4-Boc and a P1′-nitrile group. However, compound **5h** displayed a potent antiviral EC_{50} of 0.8 μM, over 2-fold enhancement of antiviral activity over nirmatrelvir, and over 40-fold improvement of activity over the related nitrile derivative **5b** (entries 3, 9).

Incorporation of trifluoroacetamide in combination with the keto-benzothiazole P1′-group improved Mpro activity for compound **5i**. This compound also maintained comparable antiviral activity as compound **5h** (entry 10). Incorporation of 6-membered lactam resulted in a very potent inhibitor **5j**, exhibiting an Mpro inhibitory K_i of 1.2 nM and antiviral EC_{50} value of 0.36 μM, nearly 5-fold improvement of antiviral activity compared to nirmatrelvir (entries 1 and 11). The result is consistent with our previous observation that the 6-membered P1-lactam enhances both protease inhibitory and antiviral activity compared to the 5-membered lactam.[44]

We further examined the effect of the tetrahydroisoquinoline-2-carboxamide group in compound **5k**, which showed significant loss of *in vitro* activity compared to the 3-carboxamide P2-ligand in compound **5j**. We further examined the effect of P1′-phenylthiazole in compounds **5l** and **5m** containing a P4-Boc group and P4 trifluoroacetamide group, respectively. Compound **5l** showed a comparable Mpro K_i value and antiviral activity with the corresponding benzothiazole derivative **5h** (entries 9 and 13). The trifluoroacetamide P4 ligand significantly improved Mpro inhibitory K_i for compound **5m**, however, the antiviral activity was not improved (entry 14). Incorporation of a 6-membered P1′ lactam in place of 5-membered lactam in compound **5n** resulted in reduction of K_i value but maintained similar antiviral EC_{50} values as **5m** (entries 14 and 15). We then examined the effect of the P4 group, 4-methoxy-indole-2-carboxamide in combination with P1′-nitrile and P1 6-membered lactam moieties. The resulting compound **5o** showed significant reduction of both K_i and antiviral EC_{50} values (entry 16). Derivatives **5p** and **5q** with a P1-keto phenyl thiazole in combination with 5- and 6-membered lactams showed no significant improvement of Mpro inhibitory activity over **5m** or **5n** (entries 17 and 18).

At first glance, there is high variability in the ratios of Mpro inhibitory K_i or IC_{50} values to antiviral EC_{50} values observed in Table 1. However, this variability is consistent with the variability in reported ratios published throughout the literature.[9–11,23,24] Compound **5d**, which has an EC_{50} value of 2200 nM which is similar to that of nirmatrelvir at 2000 nM, has a K_i value of 3.2 nM which is 12 times weaker than nirmatrelvir. The antiviral activity of **5h** (EC_{50} 800 nM) is about 5 times higher than the Mpro inhibitory K_i value. Compound **5j**, which has a K_i value of 1.2 nM, has a 30-fold difference from its antiviral EC_{50} value, whereas nirmatrelvir (K_i 0.26 nM) has a difference of 77-fold. Certainly, nirmatrelvir appears to have a relatively poor EC_{50} value compared to its subnanomolar K_i value. It seems reasonable that the antiviral assays which determine the EC_{50} values for compounds are subject to more variability due to differences in the compounds' ability to act as substrates for P-glycoprotein or bind to serum albumin for example. These differences can dramatically affect the free concentration of the compound available to the cells to inhibit viral replication. Also, nirmatrelvir is subject to metabolism by CYP3A4 and therefore it has to be administered to humans *via* combination with ritonavir as Paxlovid®.[32,33]

As outlined in Table 1, we have developed a new class of potent SARS-CoV-2 Mpro inhibitors. Several of these compounds blocked the replication of SARS-CoV-2 in VeroE6 cells with EC_{50} values comparable to or lower than the

approved drug, nirmatrelvir. Of particular importance, there are reports that nirmatrelvir-resistant SARS-CoV-2 3CLpro enzymes can be generated *via* different *in vitro* methods, and that some naturally occurring Mpro variants have been identified from patient samples, most notably at E166 (ref. 46, 47) and S144.[48–50] Future studies will determine whether these current inhibitors will be able to overcome naturally occurring Mpro variants such as E166, S144, or other variants identified in the patient population. Development of drug-resistance strains by *in vitro* or *in vivo* methods is considered gain-of-function studies, and such studies are suspended in the US. Therefore, future studies will likely have to rely on biochemical studies with the isolated enzyme.

To gain molecular insight into the ligand-binding site interactions of inhibitors incorporating the tetrahydroisoquinoline scaffold in combination with other P1, P1′ and P3 ligands, we determined several X-ray structures of inhibitor SARS-CoV-2 Mpro complexes during the course of our iterative design process. The X-ray structures of inhibitor **5c**, **5j** and **5m** bound Mpro were determined to 1.2 to 1.8 Å in resolution (see Table S1, SI section). Our X-ray crystallographic data clearly showed strong and continuous electron density for all inhibitors in the Mpro active site. The polder electron density omit maps surrounding compounds **5c**, **5j**, and **5m** are shown in the supplementary data section. The main difference between inhibitor **5c** and nirmatrelvir is that the bicyclic proline is replaced with a conformationally constrained tetrahydroisoquinoline scaffold in inhibitor **5c**. The overall structure of **5c** shows a lot of resemblance to the nirmatrelvir-bound SARS- CoV-2 Mpro complex.[28,40] The key interactions between inhibitor **5c** and the SARS- CoV-2 Mpro active site are represented in Fig. 3. Inhibitor **5c** occupies the Mpro active site from S1 to S4 subsites, forming seven direct hydrogen bonds with the residue in the active site. Both P1′ nitrile and P1 lactam functionalities of inhibitor **5c** show similar hydrogen bonding interactions to nirmatrelvir. As can be seen, the nucleophilic attack by the active site Cys145 sulfur on the P1′ nitrile functionality led to the formation of an imidate which forms a hydrogen bond with the Cys145 backbone NH.

The P1 5-membered lactam also forms two strong hydrogen bonds with the backbone carbonyl of Phe140 and the side chain carboxylate of Glu166. The lactam carbonyl group, on the other hand, forms a strong hydrogen bond with the presumably protonated His163 side chain imidazole nitrogen. Furthermore, the P2 amide NH forms a hydrogen bond with the backbone carbonyl of His164. The P3 amide carbonyl group and the P4 amide NH form two hydrogen bonds with the Glu166 backbone carbonyl and the side chain carboxylate, respectively. The THIQ fused bicyclic scaffold appears to nestle in the S3 hydrophobic pockets and is involved in the formation of van der Waals interactions in this region. These interactions are highlighted in Fig. 4.

Interestingly, the P2 THIQ amide NH forms a strong hydrogen bond with the His164 backbone carbonyl group (2.7 Å for **5c** *vs.* 3.0 Å for nirmatrelvir) compared to nirmatrelvir. The flat aromatic ring of THIQ appears to engage in extensive van der Waals interactions in the S2 subsite, particularly with His41, Met49, Tyr 54, Arg188, and Glu189. These interactions along with strong hydrogen bond interaction may have contributed towards the high affinity of inhibitor **5c**. An overlay of the X-ray structures of **5c**-bound SARS-CoV-2 Mpro and nirmatrelvir-bound SARS-CoV-2 Mpro is shown in Fig. 5. The structure reveals that the THIQ ligand effectively occupies the S2 subsite over the cyclopropylproline scaffold of nirmatrelvir. Based upon this structural analysis, we speculated that with appropriate combination of P1 and P1′ ligands, inhibitor activity can be further improved.

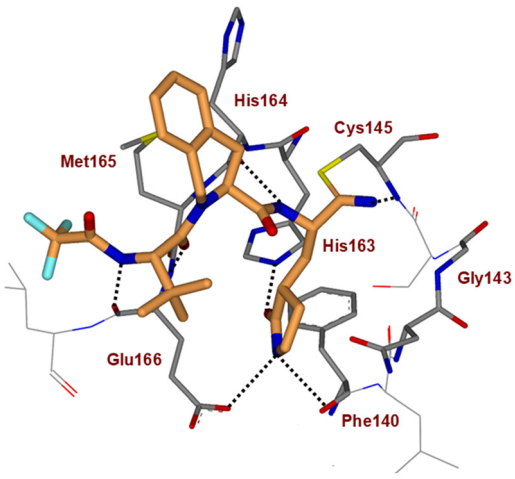

Fig. 3 X-ray structure of inhibitor **5c**-bound (GRL-05122) SARS-CoV-2 Mpro. The inhibitor carbon atoms are shown in orange and the Mpro carbon atoms are shown in grey. Hydrogen bond interactions between **5c** and Mpro are indicated by dotted lines (PDB ID:9E7S).

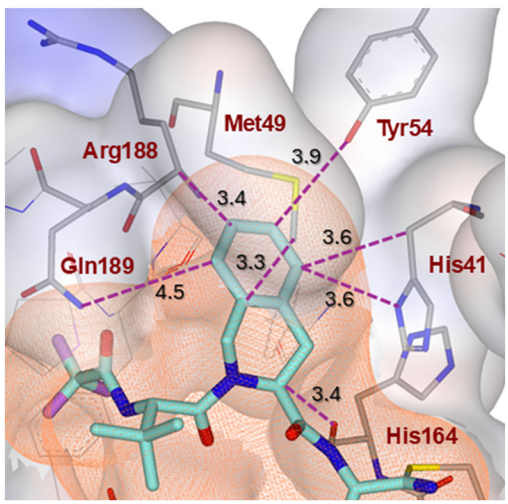

Fig. 4 Interactions of the P2 tetrahydroisoquinoline-3-carboxamide in the S1–S2 subsites. Various van der Waals interactions and distances from the selected residues are shown (magenta dashed lines).

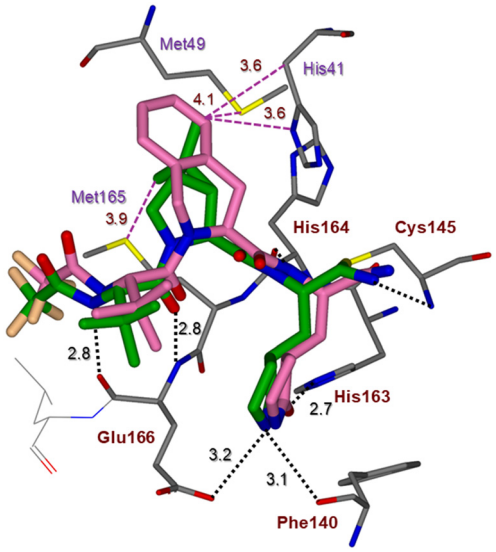

Fig. 5 Overlay of X-ray structures of **5c** (carbon atoms, magenta)-bound SARS-CoV-2 Mpro and nirmatrelvir (carbon atoms, green)-bound SARS-CoV-2 Mpro. The P2 groups of both compounds form extensive van der Waals interactions in the S2 subsite. The distances of cyclopropyl proline from the selected residues are shown (dashed magenta lines).

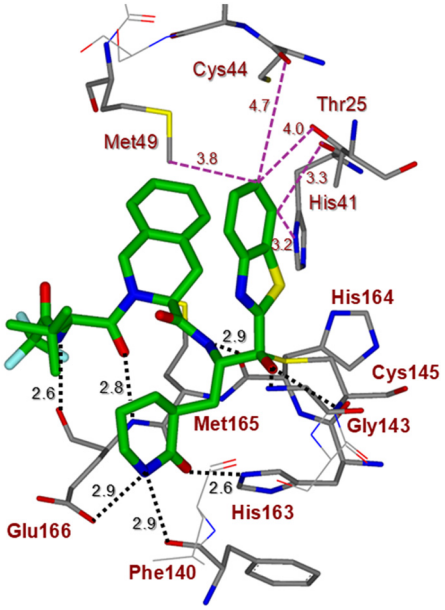

Fig. 6 X-ray crystal structure of SARS-CoV-2 Mpro covalently bound to compound **5j** (GRL-06222) (carbon green) through Cys145 (PDB: 9ZO3). The benzothiazole ligand forms extensive van der Waals interactions in the S1′ subsite. P1 six-membered lactam forms strong hydrogen bonds (black dotted lines).

We investigated inhibitors containing the THIQ P2 ligand in combination with the P1′ keto-thiazole group and P1 5- and 6 membered lactam ligands. Among these combinations, inhibitor **5j** with a 6-membered P1 lactam and benzothiazole P1′ group resulted in very potent inhibitor **5j**. This compound is the most potent compound in this series, showing nearly 3-fold improvement of Mpro activity and 100-fold antiviral activity over inhibitor **5c**. Inhibitor **5j** also shows over 5-fold improvement of antiviral activity compared to nirmatrelvir in the same assays. The X-ray structure of **5j**-bound SARS-CoV-2 Mpro was determined and the active site interactions are depicted in Fig. 6. The inhibitor fully occupied the active site forming eight direct hydrogen bonds with the residues in the active site. The ligand-binding interactions of the P1, P3 and P4 groups in the Mpro active site are similar to inhibitor **5c** and nirmatrelvir. In the S1 subsite, the sulfur atom of Cys145 formed a covalent bond with the carbonyl carbon adjacent to benzothiazole heterocycles. This resulted in the formation of a direct hydrogen bond and in a water-mediated hydrogen bonding interaction around the oxyanion hole residues, Cys145 and Gly143. Interestingly, the benzothiazole benzene ring nestles in the hydrophobic pocket surrounding the His41 side chain, His41 backbone, Thr25 side chain, Met49 side chain, and Cys44 backbone. Overall, hydrophobic elements such as the THIQ template, the six-membered lactam, and the benzothiazole heterocycle contributed to the Mpro inhibitor's affinity *via* extensive van der Waals interactions. In addition, the high lipophilicity of compound **5j** (clog*P* 4.0) compared to **5c** (clog*P* 0.9) may have contributed towards the significant improvement of antiviral activity.[51,52]

The active site interactions of phenylthiazole inhibitor **5m** bound to SARS-CoV-2 Mpro are shown in Fig. 7. The main difference between **5j** and **5m** is the presence of a P1′ phenylthiazole heterocycle. Like the benzothiazole-derived inhibitor **5j**, inhibitor **5m** occupied the Mpro active site from S1 to S4 subsites. It formed seven direct hydrogen bonds with

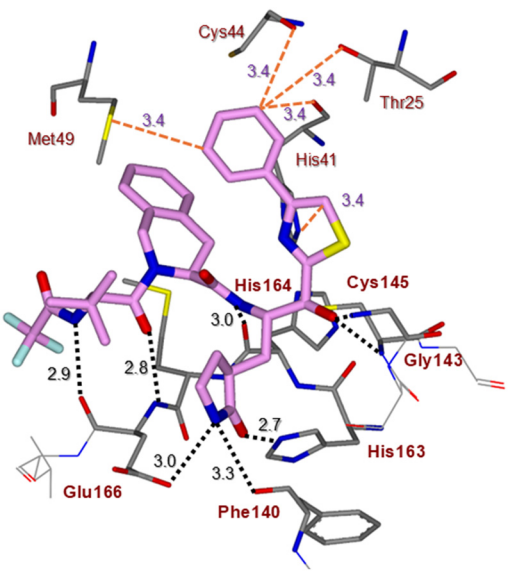

Fig. 7 X-ray crystal structure of SARS-CoV-2 Mpro covalently bound to compound **5m** (GRL-05022) (carbon magenta) through Cys145 (PDB:9ZNL). The phenylthiazole ligand forms van der Waals interactions in the S1′ subsite. The P1 five-membered lactam forms multiple hydrogen bonds (black dotted lines).

the active site residues. Most of the active site interactions are similar to the benzothiazole-derived compound **5j**. The van der Waals interactions in the S1′ subsite are mostly similar. Interestingly, the six- membered P1 lactam forms a stronger hydrogen bond with the Glu166 side chain, Phe140 backbone carboxyl and His163 side chain. This may explain the slightly better Mpro inhibitory activity of **5j** compared to **5m**. Compound **5j** however showed over 7-fold antiviral activity improvement compared to compound **5m**.

Conclusions

In conclusion, we designed a new class of highly potent SARS-CoV-2 Mpro inhibitors. These inhibitors incorporated conformationally constrained tetrahydro isoquinoline carboxamide as the P2 ligand. Our investigation focused on modulation of inhibitor interactions in combination with various P1, P1′, P3 and P4′ ligands of nirmatrelvir. In particular, we examined nitrile and substituted keto-benzothiazoles as the P1′ ligand in combination with P2 THIQ-carboxamides and P4 urea, trifluoroacetamide, carbamate, substituted indole carboxamide derivatives. In addition, we examine the effect of P3 *tert*-butyl and iso-propyl groups in our studies. Several compounds containing the THIQ scaffold and a specific combination of other ligands exhibited excellent SARS-CoV-2 Mpro inhibitory activity and antiviral activity in veroE6 cells. In general, THIQ-3-carboxamides showed more favorable *in vitro* activity than the corresponding THIQ-2-carboxamide derivatives. Compounds **5h** and **5j** exhibited antiviral potency, with EC_{50} values of 800 nM and 360 nM, respectively. They are more potent than the FDA approved drug nirmatrelvir. To assess the ligand binding site interactions of the P2 THIQ-carboxamide ligand in the S2 subsite, we determined the high resolution X-ray crystal structures of inhibitors **5c**, **5j**, **5m**-bound to SARS-CoV-2 Mpro. Our structural analysis indicated that the tetrahydroisoquinoline carboxamide formed very strong hydrogen bonds with the backbone amide NH of Glu166. The tetrahydro isoquinoline heterocycle also fills the S2 hydrophobic pocket more effectively than nirmatrelvir's bicyclic proline moiety. The current results will pave the way for further optimization of the tetrahydro isoquinoline-derived SARS-CoV-2 Mpro inhibitors. Structure-based design and further optimization of this class of inhibitors are in progress in our laboratories.

Experimental

All chemicals and solvents were purchased from commercial suppliers and were used as received unless otherwise stated. All reactions were carried out under an argon atmosphere in either flame or oven-dried (120 °C) glassware. TLC analysis was conducted using glass-backed thin-layer silica gel chromatography plates (60 Å, 250 μm thickness, F254 indicator). Column chromatography was performed using silica gel, 230–400 mesh, 60 Å pore diameter. Isolated yields were determined following purification. Proton Nuclear Magnetic Resonance NMR (^{1}H NMR) spectra and carbon nuclear magnetic resonance (^{13}C NMR) spectra were recorded on Bruker AV-III-400HD and Bruker AVIII-800 spectrometers. Chemical shifts for protons are reported in parts per million and are referenced to the NMR solvent peak ($CDCl_3$: δ 7.26). Chemical shifts for carbons are reported in parts per million and are referenced to the carbon resonances of the NMR solvent ($CDCl_3$: δ 77.16). Data are reported as (s = singlet, d = doublet, t = triplet, q = quartet, quint = quintet, sep = septet, m = multiplet, dd = doublet of doublets, ddd = doublet of doublet of doublets, dddd = doublet of doublet of doublets of doublets, td = triplet of doublets, dq = doublet of quartets, qd = quartet of doublets, dt = doublet of triplets, brs = broad singlet). All coupling constants are measured in hertz (Hz). High-resolution mass spectrometry (HRMS) spectra were recorded under positive electron spray ionization (ESI^+) on an Agilent 6550 Q-TOF LC/MS instrument at the Purdue University Analytical Mass Spectrometry Facility.

tert-Butyl((*S*)-1-(benzo[*d*]thiazol-2-yl)-1-oxo-3-((*S*)-2-oxopyrrolidin-3-yl)propan-2-yl)carbamate (12a)

To the stirred solution of benzothiazole (420 mg, 3.1 mmol) in anhydrous THF (10 mL) at −78 °C, *n*-BuLi (1.2 M solution in hexane, 2.3 mL, 2.8 mmol) was added dropwise. After stirring the reaction mixture at the same temperature for 45 min, compound **11a** (250 mg, 0.8 mmol) dissolved in 4 mL of THF was added dropwise. After 3 h, the reaction was quenched with NH_4Cl and extracted with EtOAc (3×). The combined organic layers were washed with brine, dried over Na_2SO_4, filtered, and concentrated under reduced pressure. Purification by silica gel column chromatography (2% MeOH/CH_2Cl_2) afforded compound **12a** (200 mg, 64% yield) as an amorphous white solid. ^{1}H NMR (500 MHz, CDCl3) δ 8.17 (d, J = 8.5 Hz, 1H), 7.98 (d, J = 7.9 Hz, 1H), 7.55 (dd, J = 12.0, 7.7 Hz, 2H), 6.12 (s, 1H), 5.85 (s, 1H), 5.67–5.52 (m, 1H), 3.43–3.28 (m, 2H), 2.71–2.45 (m, 2H), 2.25–1.95 (m, 3H), 1.43 (s, 9H); ^{13}C NMR (101 MHz, $CDCl_3$) δ 193.2, 179.8, 163.7, 155.7, 153.4, 137.1, 127.9, 127.0, 125.6, 122.3, 79.8, 55.3, 40.4, 38.5, 34.5, 28.2, 27.9. LRMS-ESI (m/z): 390 $[M + H]^+$.

tert-Butyl((*S*)-1-(benzo[*d*]thiazol-2-yl)-1-oxo-3-((*S*)-2-oxopiperidin-3-yl)propan-2-yl)carbamate (12b)

Compound **12b** is synthesized by using the same procedure used for the synthesis of compound **12a.** Compound **11b** (250 mg, 0.75 mmol) afforded compound **12b** (180 mg, 60% yield) as an amorphous white solid. ^{1}H NMR (500 MHz, $CDCl_3$) δ 8.15 (d, J = 8.1 Hz, 1H), 7.96 (d, J = 7.9 Hz, 1H), 7.59–7.48 (m, 2H), 6.31 (s, 1H), 5.93 (d, J = 8.3 Hz, 1H), 5.60 (s, 1H), 3.30 (dt, J = 13.4, 7.1 Hz, 2H), 2.53 (d, J = 8.7 Hz, 1H), 2.36–2.21 (m, 2H), 2.12 (d, J = 11.0 Hz, 1H), 1.99–1.87 (m, 1H), 1.85–1.73 (m, 2H), 1.43 (s, 9H); ^{13}C NMR (126 MHz, $CDCl_3$) δ 193.6, 174.6, 164.1, 155.9, 153.5, 137.3, 127.8, 127.0, 125.6, 122.4, 79.9, 54.9, 42.4, 38.5, 34.7, 28.3, 26.5, 21.5. LRMS-ESI

(*m*/*z*): 404 $[M + H]^+$. HRMS (ESI): *m*/*z* calcd for $C_{20}H_{26}N_3O_4S$ $[M + H]^+$ 404.1644 found 404.1653.

tert-Butyl((*S*)-1-oxo-3-((*S*)-2-oxopyrrolidin-3-yl)-1-(4-phenylthiazol-2-yl)propan-2-yl)carbamate (13a)

To the stirred solution of 4-phenylthiazole (470 mg, 3.1 mmol) in anhydrous THF (10 mL) at −78 °C, *n*-BuLi (1.2 M solution in hexane, 2.3 mL, 2.8 mmol) was added dropwise. After stirring the reaction mixture at the same temperature for 45 min, compound **11a** (244 mg, 0.77 mmol) dissolved in 4 mL of THF was added dropwise. After 3 h, the reaction was quenched with NH_4Cl and extracted with EtOAc (3×). The combined organic layers were washed with brine, dried over Na_2SO_4, filtered, and concentrated under reduced pressure. Purification by silica gel column chromatography (2% MeOH/CH_2Cl_2) afforded compound **13a** (230 mg, 72% yield) as an amorphous white solid. ^{1}H NMR (500 MHz, $CDCl_3$) δ 7.98–7.79 (m, 3H), 7.50–7.30 (m, 3H), 6.54 (s, 1H), 5.76 (d, *J* = 8.7 Hz, 1H), 5.57 (s, 1H), 3.45–3.26 (m, 2H), 2.69–2.53 (m, 2H), 2.22–1.95 (m, 3H), 1.44 (s, 9H); ^{13}C NMR (126 MHz, $CDCl_3$) δ 191.7, 179.9, 163.9, 157.7, 155.9, 133.4, 129.0, 126.4, 120.5, 80.0, 55.2, 40.4, 38.6, 35.0, 28.3, 27.9. LRMS-ESI (*m*/*z*): 416 $[M + H]^+$. HRMS (ESI): *m*/*z* calcd for $C_{21}H_{26}N_3O_4S$ $[M + H]^+$ 416.1644 found 416.1652.

tert-Butyl((*S*)-1-oxo-3-((*S*)-2-oxopiperidin-3-yl)-1-(4-phenylthiazol-2-yl)propan-2-yl)carbamate (13b)

Following the above procedure described for the preparation of **13a**, the reaction of **11b** (253 mg, 0.77 mmol) afforded compound **13b** (220 mg, 66% yield) as an amorphous white solid. ^{1}H NMR (500 MHz, $CDCl_3$) δ 7.94–7.89 (m, 2H), 7.83 (s, 1H), 7.44 (t, *J* = 7.5 Hz, 2H), 7.38 (d, *J* = 7.3 Hz, 1H), 6.45 (s, 1H), 5.82 (d, *J* = 8.6 Hz, 1H), 5.64–5.51 (m, 1H), 3.28 (dt, *J* = 20.9, 4.6 Hz, 2H), 2.59–2.50 (m, 1H), 2.42–2.31 (m, 1H), 2.25 (d, *J* = 11.2 Hz, 1H), 2.18–2.06 (m, 1H), 1.93 (dt, *J* = 8.5, 4.0 Hz, 1H), 1.85–1.73 (m, 2H), 1.43 (s, 9H); ^{13}C NMR (126 MHz, $CDCl_3$) δ 192.0, 174.6, 164.1, 157.5, 156.0, 133.5, 128.9, 128.9, 126.4, 120.3, 79.9, 54.7, 42.4, 38.4, 34.9, 28.3, 26.2, 21.4. LRMS-ESI (*m*/*z*): 430 $[M + H]^+$. HRMS (ESI): *m*/*z* calcd for $C_{22}H_{28}N_3O_4S$ $[M + H]^+$ 430.1801 found 430.1808.

Synthesis of dipeptide compounds (14a–14d, 17, procedure A)

To the stirred solution of (*S*)-methyl 1,2,3,4-tetrahydroisoquinoline-3-carboxylate hydrochloride (amine **9**) (1.0 equiv.) in DMF at °C were added *N*-*tert*-butylformamide-L-*tert*-leucine (**8a**) (1.0 equiv.), *N*-Boc-L-*tert*-leucine (**8b**) (1.0 equiv.), *N*-Boc-L-valine (**8c**) (1.0 equiv.) and *N*-Boc-L-leucine (**8d**) (1.0 equiv.) After stirring the reaction mixture for 5 min, HATU (1.2 equiv.) was added followed by DIPEA (3.0 equiv.). After 10 minutes, the ice bath was removed, and the reaction mixture was stirred at 23 °C for 12 h. The solvent was then evaporated under high vacuum, and the residue was dissolved in ethyl acetate. The organic layer was washed with water, 1 N HCl, and brine, dried over Na_2SO_4, concentrated under reduced pressure and the residue was purified by column chromatography (10–30% EtOAc/hexane) to give the corresponding dipeptide esters **14a–14d** in excellent yields. Similarly, by following the same procedure coupling of *N*-Boc-L-*tert*-leucine (**8b**) with (*S*)-methyl 1,2,3,4-tetrahydroisoquinoline-1-carboxylate hydrochloride (**16**) provided dipeptide **17** in good yield.

Methyl (*S*)-2-((*S*)-2-(3-(*tert*-butyl)ureido)-3,3-dimethylbutanoyl)-1,2,3,4-tetrahydroisoquinoline-3-carboxylate (14a). The reaction was conducted according to general procedure **A**. To the stirred solution of (*S*)-methyl 1,2,3,4-tetrahydroisoquinoline-3-carboxylate hydrochloride **9** (250 mg, 1.1 mmol) in DMF (5 mL) at 0 °C were added **8a** (253 mg, 1.1 mmol), HATU (500 mg, 1.32 mmol) and DIPEA (0.6 mL, 3.3 mmol). Purification by silica gel column chromatography (30% EtOAc/hexane) afforded the dipeptide **14a** (350 mg, 78% yield) as a white solid. The analytical HPLC purity of compound **14a** was determined by using an HPLC-Agilent 1260 infinity (VYDAC, protein and peptide C18), 50% ACN/H_2O, 0.5 mL min^{-1}, t_r: 14.98 min, purity = 99%. ^{1}H NMR (500 MHz, $CDCl_3$) δ 7.18–7.04 (m, 4H), 5.57 (d, *J* = 9.4 Hz, 1H), 5.30 (t, *J* = 5.4 Hz, 1H), 5.06 (d, *J* = 15.3 Hz, 1H), 4.93 (d, *J* = 9.4 Hz, 1H), 4.85 (s, 1H), 4.72 (d, *J* = 15.3 Hz, 1H), 3.57 (s, 3H), 3.17 (dd, *J* = 15.6, 5.1 Hz, 1H), 3.08 (d, *J* = 5.9 Hz, 1H), 1.21 (s, 9H), 1.06 (s, 9H); ^{13}C NMR of major rotamer (126 MHz, $CDCl_3$) δ 173.3, 171.5, 157.1, 132.7, 132.4, 127.9, 127.3, 127.1, 126.3, 55.6, 52.6, 52.2, 50.1, 46.7, 36.4, 31.1, 29.5, 26.6. LRMS-ESI (*m*/*z*): 404 $[M + H]^+$. HRMS (ESI): *m*/*z* calcd for $C_{22}H_{34}N_3O_4$ $[M + H]^+$ 404.2549 found 404.2554.

Methyl (*S*)-2-((*S*)-2-((*tert*-butoxycarbonyl)amino)-3,3-dimethylbutanoyl)-1,2,3,4-tetrahydroisoquinoline-3-carboxylate (14b). The reaction was conducted according to general procedure **A**. To the stirred solution of (*S*)-methyl 1,2,3,4-tetrahydroisoquinoline-3-carboxylate hydrochloride **9** (500 mg, 2.20 mmol) in DMF (10 mL) at 0 °C were added *N*-Boc-L-*tert*-leucine (**8b**) (510 mg, 2.20 mmol), HATU (1.0 g, 2.64 mmol) and DIPEA (1.2 mL, 6.6 mmol). Purification by silica gel column chromatography (15% EtOAc/hexane) afforded the dipeptide **14b** (808 mg, 91% yield) as a white solid. The analytical HPLC purity of compound **14b** was determined by using an HPLC-Agilent 1260 infinity (VYDAC, protein and peptide C18), 50% ACN/H_2O, 0.8 mL min^{-1}, t_r: 15.48 min, purity = 99%. ^{1}H NMR of major rotamer (500 MHz, $CDCl_3$) δ 7.21 (td, *J* = 6.2, 3.5 Hz, 2H), 7.15 (dd, *J* = 9.3, 5.8 Hz, 2H), 5.43–5.37 (m, 1H), 5.33 (dd, *J* = 9.8, 3.7 Hz, 1H), 5.00 (d, *J* = 15.2 Hz, 1H), 4.76–4.64 (m, 2H), 3.60 (s, 3H), 3.23 (dd, *J* = 15.7, 4.7 Hz, 1H), 3.13 (dd, *J* = 15.7, 6.0 Hz, 1H), 1.40 (s, 9H), 1.08 (s, 9H); ^{13}C NMR of major rotamer (126 MHz, $CDCl_3$) δ 172.1, 171.4, 155.6, 132.5, 132.4, 128.1, 127.4, 127.1, 126.3, 79.6, 56.6, 52.3, 46.7, 36.4, 30.9, 28.4, 26.4. LRMS-ESI (*m*/*z*): 405 $[M + H]^+$; HRMS (ESI): *m*/*z* calcd for $C_{22}H_{33}N_2O_5$ $[M + H]^+$ 405.2389 found 405.2398.

Methyl (*S*)-2-((*tert*-butoxycarbonyl)-L-valyl)-1,2,3,4-tetrahydroisoquinoline-3-carboxylate (14c). The reaction was conducted according to general procedure **A**. To the stirred solution of (*S*)-methyl 1,2,3,4-tetrahydroisoquinoline-3-carboxylate hydrochloride **9** (500 mg, 2.2 mmol) in DMF (10

mL) at 0 °C were added **8c** (477 mg, 2.2 mmol), HATU (1.0 g, 2.64 mmol) and DIPEA (1.2 mL, 6.6 mmol). Purification by silica gel column chromatography (16% EtOAc/hexane) afforded compound **14c** (763 mg, 89% yield) as a white solid. The analytical HPLC purity of compound **14c** was determined by using an HPLC-Agilent 1260 infinity (VYDAC, protein and peptide C18), 50% ACN/H_2O, 0.5 mL min^{-1}, t_r: 18.25 min, purity = 99%. ^1H NMR of major rotamer (400 MHz, $CDCl_3$) δ 7.24–7.17 (m, 2H), 7.15 (td, J = 10.2, 5.5 Hz, 2H), 5.40 (t, J = 5.2 Hz, 1H), 5.30 (d, J = 9.1 Hz, 1H), 4.92 (d, J = 15.0 Hz, 1H), 4.75–4.53 (m, 2H), 3.62 (s, 3H), 3.22 (d, J = 4.7 Hz, 1H), 3.15 (d, J = 6.0 Hz, 1H), 2.13 (q, J = 6.6 Hz, 1H), 1.41 (s, 9H), 1.08 (d, J = 6.8 Hz, 3H), 0.96 (d, J = 6.6 Hz, 3H); ^{13}C NMR of major rotamer (101 MHz, $CDCl_3$) δ 172.2, 171.1, 155.7, 132.2, 131.8, 128.2, 127.3, 127.0, 126.1, 79.5, 55.4, 52.2, 51.9, 45.6, 31.2, 30.5, 28.2, 19.4, 17.0. LRMS-ESI (m/z): 391 $[M + H]^+$; HRMS (ESI): m/z calcd for $C_{21}H_{31}N_2O_5$ $[M + H]^+$ 391.2232 found 391.2240.

Methyl (*S*)-2-((*tert*-butoxycarbonyl)-L-leucyl)-1,2,3,4-tetrahydroisoquinoline-3-carboxylate (14d). The reaction was conducted according to general procedure **A**. To the stirred solution of (*S*)-methyl 1,2,3,4-tetrahydroisoquinoline-3-carboxylate hydrochloride **9** (500 mg, 2.2 mmol) in DMF (10 mL) at °C were added **8d** (508 mg, 2.2 mmol), HATU (1.0 g, 2.64 mmol) and DIPEA (1.2 mL, 6.6 mmol). Purification by silica gel column chromatography (15% EtOAc/hexane) afforded the dipeptide **14d** (720 mg, 81% yield) as a white solid. The analytical HPLC purity of compound **14d** was determined by using an HPLC-Agilent 1260 infinity (VYDAC, protein and peptide C18), 50% ACN/H_2O, 0.5 mL min^{-1}, t_r: 24.84 min, purity = 99%. ^1H NMR of major rotamer δ 7.23–7.18 (m, 2H), 7.17–7.14 (m, 1H), 7.11 (d, J = 3.5 Hz, 1H), 5.41 (dd, J = 6.0, 4.1 Hz, 1H), 5.24 (d, J = 8.9 Hz, 1H), 4.92 (d, J = 15.2 Hz, 1H), 4.83 (td, J = 9.5, 3.9 Hz, 1H), 4.67 (d, J = 15.2 Hz, 1H), 3.61 (s, 3H), 3.23 (d, J = 4.3 Hz, 1H), 3.16 (d, J = 6.2 Hz, 1H), 1.89–1.75 (m, 1H), 1.63–1.56 (m, 1H), 1.55–1.49 (m, 1H), 1.41 (s, 9H), 1.09 (d, J = 6.5 Hz, 3H), 0.99 (d, J = 6.7 Hz, 3H); ^{13}C NMR of major rotamer (126 MHz, $CDCl_3$) δ 173.1, 171.2, 155.6, 132.2, 131.8, 128.3, 127.4, 127.1, 126.2, 79.6, 52.4, 51.9, 49.3, 45.4, 42.3, 30.7, 28.4, 24.7, 23.4, 22.0. LRMS-ESI (m/z): 405 $[M + H]^+$. HRMS (ESI): m/z calcd for $C_{22}H_{33}N_2O_5$ $[M + H]^+$ 405.2389 found 405.2398.

Methyl (*S*)-2-((*S*)-2-((*tert*-butoxycarbonyl)amino)-3,3-dimethylbutanoyl)-1,2,3,4-tetrahydroisoquinoline-1-carboxylate (17). The reaction was conducted according to general procedure **A**. To the stirred solution of amine **16** (250 mg, 1.1 mmol) in DMF (5 mL) at °C were added *N*-Boc-L-*tert*-leucine (255 mg, 1.1 mmol), HATU (500 mg, 1.32 mmol) and DIPEA (0.6 mL, 3.3 mmol). Purification by silica gel column chromatography (15% EtOAc/hexane) afforded the dipeptide **17** (346 mg, 77% yield) as a white solid. The analytical HPLC purity of compound **17** was determined by using an HPLC-Agilent 1260 infinity (VYDAC, protein and peptide C18), 47% ACN/H_2O, 0.5 mL min^{-1}, t_r: 34.73 min, purity = 97%. ^1H NMR of major rotamer (500 MHz, $CDCl_3$) δ 7.53–7.47 (m, 1H), 7.27–7.19 (m, 2H), 7.19–7.13 (m, 1H), 5.98 (s, 1H), 5.36–5.24 (m, 1H), 4.66 (d, J = 9.8 Hz, 1H), 3.97 (d, J = 6.0 Hz, 2H), 3.71 (s, 3H), 2.97 (ddd, J = 16.8, 10.7, 6.0 Hz, 2H), 1.40 (s, 9H), 1.07 (s, 9H); ^{13}C NMR of major rotamer (126 MHz, $CDCl_3$) δ 171.9, 171.0, 155.6, 134.9, 130.3, 128.4, 128.4, 127.9, 126.8, 79.5, 56.7, 56.1, 52.5, 43.1, 36.2, 29.1, 28.4, 26.4. LRMS-ESI (m/z): 405 $[M + H]^+$. HRMS (ESI): m/z calcd for $C_{22}H_{33}N_2O_5$ $[M + H]^+$ 405.2389 found 405.2400.

Methyl (*S*)-2-((*S*)-3,3-dimethyl-2-(2,2,2-trifluoroacetamido) butanoyl)-1,2,3,4-tetrahydroisoquinoline-3-carboxylate (15a). To the stirred solution of dipeptide **14b** (250 mg, 0.61 mmol) in CH_2Cl_2 (5 mL) at 23 °C were added $ZnCl_2$ (9 mg, 0.061 mmol) and TFAA (0.3 mL, 1.83 mmol). After 12 h, the reaction was quenched with H_2O and extracted with CH_2Cl_2 (3×). The combined organic layers were washed with brine, dried over Na_2SO_4, filtered, and concentrated under reduced pressure. Purification by silica gel column chromatography (20% EtOAc/hexanes) afforded compound **15a** (198 mg, 81% yield) as an amorphous white solid. The analytical HPLC purity of compound **15a** was determined by using an HPLC-Agilent 1260 infinity (VYDAC, protein and peptide C18), 50% ACN/H_2O, 0.5 mL min^{-1}, t_r: 19.59 min, purity = 99%. ^1H NMR of major rotamer (500 MHz, $CDCl_3$) δ 7.27–7.14 (m, 4H), 5.26 (t, J = 5.6 Hz, 1H), 5.05 (d, J = 9.0 Hz, 1H), 4.89 (d, J = 15.2 Hz, 1H), 4.74 (d, J = 15.0 Hz, 1H), 3.66 (s, 3H), 3.19 (dd, J = 9.0, 5.7 Hz, 2H), 1.12 (s, 9H); ^{13}C NMR of major rotamer (126 MHz, $CDCl_3$) δ 171.1, 169.8, 156.78 (q, J = 38.4 Hz), 132.5, 132.0, 128.1, 127.8, 127.3, 126.1, 119.3–112.4 (m), 55.9, 53.1, 52.4, 46.9, 37.2, 30.8, 26.4. LRMS-ESI (m/z): 401 $[M + H]^+$. HRMS (ESI): m/z calcd for $C_{19}H_{24}F_3N_2O_4$ $[M + H]^+$ 401.1688 found 401.1699.

Methyl (*S*)-2-((2,2,2-trifluoroacetyl)-L-valyl)-1,2,3,4-tetrahydroisoquinoline-3-carboxylate (15b). To the stirred solution of dipeptide **14c** (240 mg, 0.61 mmol) in CH_2Cl_2 (5 mL) at 23 °C were added $ZnCl_2$ (9 mg, 0.061 mmol) and TFAA (0.3 mL, 1.83 mmol). After 12 h, the reaction was quenched with H_2O and extracted with CH_2Cl_2 (3×). The combined organic layers were washed with brine, dried over Na_2SO_4, filtered, and concentrated under reduced pressure. Purification by silica gel column chromatography (18% EtOAc/hexanes) afforded compound **15b** (180 mg, 76% yield) as an amorphous white solid. The analytical HPLC purity of compound **15b** was determined by using an HPLC-Agilent 1260 infinity (VYDAC, protein and peptide C18), 50% ACN/H_2O, 0.5 mL min^{-1}, t_r: 14.45 min, purity = 99%. ^1H NMR of rotamer mixture (500 MHz, $CDCl_3$) δ 7.74–7.61 (m, 1H), 7.24–7.19 (m, 2H), 7.18–7.12 (m, 2H), 5.34–5.29 (m, 1H), 5.05–4.95 (m, 1H), 4.93–4.80 (m, 1H), 4.79–4.70 (m, 1H), 3.63 (m, 3H), 3.32–3.08 (m, 2H), 2.37–2.04 (m, 1H), 1.14–0.98 (m, 6H); ^{13}C NMR of rotamers mixture (126 MHz, $CDCl_3$) δ 170.9, 170.4, 157.4–157.0 (m), 132.2, 131.6, 128.3, 127.7, 127.3, 126.2, 119.3–112.5 (m), 54.9, 52.6, 52.4, 45.9, 31.5, 30.6, 19.3, 17.3. LRMS-ESI (m/z): 387 $[M + H]^+$. HRMS (ESI): m/z calcd for $C_{18}H_{22}F_3N_2O_4$ $[M + H]^+$ 387.1532 found 387.1539.

Methyl (*S*)-2-((S)-3,3-dimethyl-2-(2,2,2-trifluoroacetamido) butanoyl)-1,2,3,4tetrahydroisoquinoline-1-carboxylate (18). To

the stirred solution of dipeptide **17** (250 mg, 0.61 mmol) in CH_2Cl_2 (5 mL) at 23 °C were added $ZnCl_2$ (9 mg, 0.061 mmol) and TFAA (0.3 mL, 1.83 mmol). After 12 h, the reaction was quenched with H_2O and extracted with CH_2Cl_2 (3×). The combined organic layers were washed with brine, dried over Na_2SO_4, filtered, and concentrated under reduced pressure. Purification by silica gel column chromatography (18% EtOAc/hexanes) afforded compound **18** (180 mg, 73% yield) as an amorphous white solid. The analytical HPLC purity of compound **18** was determined by using an HPLC-Agilent 1260 infinity (VYDAC, protein and peptide C18), 50% ACN/H_2O, 0.5 mL min^{-1}, t_r: 20.37 min, purity = 99%. ^1H NMR of major rotamer (500 MHz, $CDCl_3$) δ 7.56–7.44 (m, 1H), 7.31–7.23 (m, 2H), 7.19–7.08 (m, 2H), 5.94 (s, 1H), 5.03 (d, J = 9.3 Hz, 1H), 4.10–3.97 (m, 1H), 3.95–3.86 (m, 1H), 3.73 (s, 3H), 3.10–2.98 (m, 1H), 2.98–2.86 (m, 1H), 1.11 (s, 9H); ^{13}C NMR of major rotamer (126 MHz, $CDCl_3$) δ 170.7, 169.7, 156.7 (q, J = 37.1 Hz), 134.5, 129.7, 128.4, 128.3, 128.2, 127.0, 117.0–114.7 (m), 57.1, 55.5, 52.7, 43.4, 37.0, 28.9, 26.4. LRMS-ESI (m/z): 401 $[M + H]^+$. HRMS (ESI): m/z calcd for $C_{19}H_{24}F_3N_2O_4$ $[M + H]^+$ 401.1688 found 401.1699.

Methyl (*S*)-2-((4-methoxy-1*H*-indole-2-carbonyl)-L-leucyl)-1,2,3,4-tetrahydroisoquinoline-3-carboxylate (20). To a solution of compound **14d** (200 mg, 0.49 mmol) in CH_2Cl_2 (5 mL) at 0 °C was added trifluoroacetic acid (1.5 mL) and the solution was stirred for 2 h at 23 °C. After evaporating the solvent under reduced pressure the deprotected amine residue (300 mg, crude) was obtained. To the stirred solution of crude amine (300 mg, crude) in DMF (5 mL) at °C were added 4-methoxy-1*H*-indole-2-carboxylic acid (94 mg, 0.49 mmol), HATU (220 mg, 0.58 mmol) and DIPEA (0.3 mL, 1.47 mmol). The reaction mixture was stirred at 23 °C for 12 h. The solvent was then evaporated under high vacuum, and the residue was dissolved in ethyl acetate. The organic layer was washed with water, 1 N HCl, and brine, dried over Na_2SO_4, concentrated under reduced pressure and the residue was purified by silica gel column chromatography (35% EtOAc/hexanes) affording compound **20** (145 mg, 62% yield) as a white solid. The analytical HPLC purity of compound **20** was determined by using an HPLC-Agilent 1260 infinity (VYDAC, protein and peptide C18), 50% ACN/H_2O, 0.5 mL min^{-1}, t_r: 20.58 min, purity = 97%. ^1H NMR (500 MHz, $CDCl_3$) δ 10.06 (d, J = 13.3 Hz, 1H), 7.58 (d, J = 8.6 Hz, 1H), 7.21–7.12 (m, 5H), 7.11–7.08 (m, 1H), 7.06–7.02 (m, 1H), 6.99 (d, J = 8.3 Hz, 1H), 6.45 (d, J = 7.8 Hz, 1H), 5.50–5.47 (m, 1H), 5.05 (d, J = 15.0 Hz, 1H), 4.76 (d, J = 15.2 Hz, 1H), 3.90 (s, 3H), 3.61 (s, 3H), 3.28–3.22 (m, 1H), 3.19–3.12 (m, 1H), 1.97–1.84 (m, 1H), 1.81–1.76 (m, 2H), 1.10 (d, J = 6.5 Hz, 3H), 0.99 (d, J = 6.6 Hz, 3H); ^{13}C NMR of major rotamer (126 MHz, $CDCl_3$) δ 172.9, 171.2, 161.6, 154.3, 138.1, 132.1, 131.6, 129.0, 128.3, 127.4, 127.2, 126.2, 125.2, 119.0, 105.1, 101.1, 99.5, 55.3, 52.4, 52.2, 48.2, 45.5, 41.7, 30.7, 24.9, 23.4, 22.1. LRMS-ESI (m/z): 478 $[M + H]^+$. HRMS (ESI): m/z calcd for $C_{27}H_{32}N_3O_5$ $[M + H]^+$ 478.2342 found 478.2352.

Synthesis of the final inhibitor (5a–5f, procedure B)

The ester compounds **14a**, **14b**, **15a**, **15b**, **18**, **20** were dissolved in the mixture of THF : H_2O (1 : 3) (0.06 M) at 0 °C, followed by addition of $LiOH{\cdot}H_2O$ (2.0 equiv.). The reaction mixtures were stirred at room temperature for 1–5 h, then concentrated under reduced pressure to remove solvents. The crude residue was dissolved in CH_2Cl_2, neutralized with 1 N HCl and extracted with CH_2Cl_2 (3×). The combined organic layers were washed with brine, dried over Na_2SO_4, filtered, and concentrated under reduced pressure to afford the corresponding acids, which were used directly for the next step without purification.

To a solution of amine **7a**, **7b**, **12a**, **12b**, **13a**, **13b** (1 equiv.) in CH_2Cl_2 (0.05 M) at 0 °C was added trifluoroacetic acid (30 equiv.) and the solution was stirred for 2 h at 23 °C. After evaporating the solvent under reduced pressure, the corresponding deprotected amine residue (1 equiv.) was dissolved in DMF (0.03 M) followed by addition of the above synthesized acids (1 equiv.), HATU (1.2 equiv.), and DIPEA (1.2 equiv.) at 0 °C. After 10 minutes, the ice bath was removed, and the reaction mixture was stirred at 23 °C for 12 h. The solvent was then evaporated under high vacuum, and the residue was dissolved in EtOAc. The organic layer was washed with water, 1 N HCl, and brine, dried over Na_2SO_4, concentrated under reduced pressure and the residue was purified by column chromatography (1–3% MeOH/CH_2Cl_2) to give the corresponding SARS COV-2 protease inhibitors (**5a–5q**).

(*S*)-2-((*S*)-2-(3-(*tert*-Butyl)ureido)-3,3-dimethylbutanoyl)-*N*-((*S*)-1-cyano-2-((*S*)-2-oxopyrrolidin-3-yl)ethyl)-1,2,3,4-tetrahydroisoquinoline-3-carboxamide (5a). Following the ester hydrolysis procedure described in general procedure **B**, the reaction of ester **14a** (55 mg, 0.14 mmol) afforded the acid (46 mg, 88% crude) as a white fluffy solid. To a solution of amine **7a** (30 mg, 0.12 mmol) in CH_2Cl_2 (2 mL) at 0 °C was added trifluoroacetic acid (0.5 mL) and the solution was stirred for 2 h at 23 °C. After evaporating the solvent under reduced pressure, the corresponding deprotected amine residue was obtained as a TFA salt, which was coupled with the corresponding acid (46 mg, 0.12 mmol) using the same procedure **B** described above, affording compound **5a** as a white solid (31 mg, 50%). The analytical HPLC purity of compound **5a** was determined by using an HPLC-Agilent 1260 infinity (VYDAC, protein and peptide C18), 50% ACN/H_2O, 0.5 mL min^{-1}, t_r: 8.62 min, purity = 99%. ^1H NMR of major rotamer (400 MHz, $CDCl_3$) δ 9.56 (d, J = 8.0 Hz, 1H), 7.22–7.12 (m, 4H), 6.71 (s, 1H), 5.57 (d, J = 8.1 Hz, 1H), 5.24 (d, J = 17.7 Hz, 1H), 5.19–5.09 (m, 1H), 4.99–4.96 (m, 1H), 4.39 (d, J = 8.1 Hz, 1H), 4.14–4.06 (m, 1H), 3.57 (d, J = 15.9 Hz, 1H), 3.30–3.19 (m, 2H), 3.00 (dd, J = 15.9, 5.5 Hz, 1H), 2.29–2.20 (m, 2H), 2.18–2.09 (m, 1H), 1.96–1.85 (m, 1H), 1.72–1.63 (m, 1H), 1.31 (s, 9H), 1.02 (s, 9H); ^{13}C NMR of major rotamer (126 MHz, $CDCl_3$) δ 178.4, 172.6, 169.2, 158.2, 132.3, 131.3, 128.7, 127.0, 126.5, 126.2, 118.4, 57.3, 56.0, 50.7, 42.9, 40.2, 39.1, 37.5, 34.4, 34.2, 29.5, 27.9, 27.1, 26.6; HRMS

(ESI): *m*/*z* calcd for $C_{28}H_{41}N_6O_4$ $[M + H]^+$ 525.3189 found 525.3175.

***tert*-Butyl((*S*)-1-((*S*)-3-(((*S*)-1-cyano-2-((*S*)-2-oxopyrrolidin-3-yl)ethyl)carbamoyl)-3,4-dihydroisoquinolin-2(1*H*)-yl)-3,3-dimethyl-1-oxobutan-2-yl)carbamate (5b).** Following the ester hydrolysis procedure described in general procedure **A**, the reaction of ester **14b** (40 mg, 0.10 mmol) afforded the acid (32 mg, 82% crude) as a white fluffy solid. Amine **7a** (20 mg, 0.08 mmol) was deprotected and coupled with the corresponding acid (32 mg, 0.079 mmol) using the same procedure **B** described above, affording compound **5b** as a white solid (18 mg, 45%). The analytical HPLC purity of compound **5b** was determined by using an HPLC-Agilent 1260 infinity (VYDAC, protein and peptide C18), 40% ACN/H_2O, 0.7 mL min^{-1}, t_r: 15.02 min, purity = 97%. ^1H NMR of major rotamer (500 MHz, $CDCl_3$) δ 8.88 (d, J = 8.0 Hz, 1H), 7.23–7.20 (m, 2H), 7.18–7.13 (m, 2H), 6.04 (s, 1H), 5.37–5.22 (m, 1H), 5.13–5.04 (m, 1H), 4.91–4.83 (m, 1H), 4.72–4.62 (m, 2H), 4.35–4.24 (m, 1H), 3.34–3.26 (m, 2H), 3.20–3.12 (m, 2H), 2.31–2.23 (m, 2H), 2.08–1.99 (m, 1H), 1.84–1.73 (m, 2H), 1.46 (s, 9H), 1.05 (s, 9H); ^{13}C NMR of major rotamer (126 MHz, $CDCl_3$) δ 178.5, 171.4, 169.4, 156.8, 133.9, 128.6, 127.1, 127.0, 126.8, 118.2, 81.0, 57.9, 56.3, 55.7, 47.5, 43.6, 40.1, 38.9, 37.3, 34.5, 28.4, 26.9; HRMS (ESI): *m*/*z* calcd for $C_{28}H_{40}N_5O_5$ $[M + H]^+$ 526.3029 found 526.3007.

(*S*)-*N*-((*S*)-1-Cyano-2-((*S*)-2-oxopyrrolidin-3-yl)ethyl)-2-((*S*)-3,3-dimethyl-2-(2,2,2-trifluoroacetamido)butanoyl)-1,2,3,4-tetrahydroisoquinoline-3-carboxamide (5c). Following the ester hydrolysis procedure described in general procedure **B**, the reaction of ester **15a** (45 mg, 0.11 mmol) afforded the acid (30 mg, 70% crude yield) as a white fluffy solid. Amine **7a** (20 mg, 0.08 mmol) was deprotected and coupled with the corresponding acid (30 mg, 0.08 mmol) using the same procedure **B** described above, affording compound **5c** as a white solid (25 mg, 60%). The analytical HPLC purity of compound **5c** was determined by using an HPLC-Agilent 1260 infinity (VYDAC, protein and peptide C18), 40% ACN/H_2O, 0.5 mL min^{-1}, t_r: 15.69 min, purity = 95%. ^1H NMR of major rotamer (500 MHz, $CDCl_3$) δ 8.26 (d, J = 7.0 Hz, 1H), 7.25–7.22 (m, 2H), 7.21–7.18 (m, 2H), 6.12 (s, 1H), 5.06 (d, J = 9.2 Hz, 1H), 4.90–4.81 (m, 2H), 4.74–4.65 (m, 1H), 4.62–4.54 (m, 1H), 3.34–3.26 (m, 2H), 3.19–3.12 (m, 2H), 2.53–2.42 (m, 1H), 2.37–2.31 (m, 1H), 2.30–2.24 (m, 1H), 1.96–1.89 (m, 1H), 1.83–1.75 (m, 1H), 1.10 (s, 9H).; ^{13}C NMR of major rotamer (126 MHz, $CDCl_3$) δ 179.5, 171.6, 169.9, 157.0–156.7 (m), 133.6, 133.5, 128.4, 127.5, 127.4, 126.0, 118.5, 118.0–114.7 (m), 56.2, 55.9, 47.9, 40.6, 39.3, 37.7, 37.1, 33.9, 31.7, 28.3, 26.4; HRMS (ESI): *m*/*z* calcd for $C_{25}H_{31}F_3N_5O_4$ $[M + H]^+$ 522.2328 found 522.2310.

(*S*)-*N*-((*S*)-1-Cyano-2-((*S*)-2-oxopiperidin-3-yl)ethyl)-2-((*S*)-3,3-dimethyl-2-(2,2,2-trifluoroacetamido)butanoyl)-1,2,3,4-tetrahydroisoquinoline-3-carboxamide (5d). Following the ester hydrolysis procedure described in general procedure **B**, the reaction of ester **15a** (40 mg, 0.10 mmol) afforded the acid (27 mg, 70% crude yield) as a white fluffy solid. Amine **7b** (20 mg, 0.074 mmol) was deprotected and coupled with the corresponding acid (32 mg, 0.079 mmol) using the same procedure **B** described above, affording compound **5d** as a white solid (20 mg, 50%). The analytical HPLC purity of compound **5d** was determined by using an HPLC-Agilent 1260 infinity (VYDAC, protein and peptide C18), 40% ACN/H_2O, 0.5 mL min^{-1}, t_r: 19.77 min, purity = 97%. ^1H of major rotamer NMR (500 MHz, $CDCl_3$) δ 8.44 (d, J = 6.6 Hz, 1H), 7.24–7.18 (m, 4H), 6.19 (s, 1H), 5.04 (d, J = 8.9 Hz, 1H), 4.96–4.88 (m, 1H), 4.85–4.80 (m, 1H), 4.73–4.61 (m, 2H), 3.38–3.25 (m, 2H), 3.20–3.10 (m, 2H), 2.53–2.40 (m, 1H), 2.31 (q, J = 5.7 Hz, 1H), 2.04–1.96 (m, 1H), 1.94–1.84 (m, 2H), 1.78–1.62 (m, 1H), 1.56–1.46 (m, 1H), 1.10 (s, 9H); ^{13}C NMR of major rotamer (126 MHz, $CDCl_3$) δ 174.4, 171.5, 169.7, 156.9–156.6 (m), 133.6, 133.4, 128.3, 127.5, 127.3, 125.9, 118.7, 118.1–114.7 (m), 56.1, 55.9, 47.8, 44.2, 42.2, 39.2, 37.2, 34.5, 31.7, 27.4, 26.4, 21.5; HRMS (ESI): *m*/*z* calcd for $C_{26}H_{33}F_3N_5O_4$ $[M + H]^+$ 536.2485 found 536.2468.

(*S*)-*N*-((*S*)-1-Cyano-2-((*S*)-2-oxopyrrolidin-3-yl)ethyl)-2-((2,2,2-trifluoroacetyl)-L-valyl)-1,2,3,4-tetrahydroisoquinoline-3-carboxamide (5e). Following the ester hydrolysis procedure described in general procedure **B**, the reaction of ester **15b** (40 mg, 0.10 mmol) afforded the acid (30 mg, 80% crude yield) as a white fluffy solid. Amine **7a** (20 mg, 0.08 mmol) was deprotected and coupled with the corresponding acid (30 mg, 0.079 mmol) using the same procedure **B** described above, affording compound **5e** as a white solid (18 mg, 45%). The analytical HPLC purity of compound **5e** was determined by using an HPLC-Agilent 1260 infinity (VYDAC, protein and peptide C18), 37% ACN/H_2O, 0.5 mL min^{-1}, t_r: 14.09 min, purity = 95%; ^1H NMR of major rotamer (500 MHz, $CDCl_3$) δ 8.41 (d, J = 6.1 Hz, 1H), 7.24–7.17 (m, 4H), 5.85 (s, 1H), 5.00 (dd, J = 8.6, 5.0 Hz, 1H), 4.80–4.75 (m, 1H), 4.74–4.68 (m, 2H), 4.65–4.51 (m, 1H), 3.40–3.30 (m, 2H), 3.22–3.15 (m, 2H), 2.37–2.31 (m, 1H), 2.29–2.17 (m, 2H), 2.00–1.94 (m, 1H), 1.87–1.78 (m, 2H), 1.11 (d, J = 6.7 Hz, 3H), 0.97 (d, J = 6.7 Hz, 3H)·; ^{13}C NMR of major rotamer (126 MHz, $CDCl_3$) δ 179.4, 171.3, 170.3, 157.2–156.9 (m), 133.4, 133.0, 128.2, 127.7, 127.3, 126.1, 118.3, 117.0–114.7 (m), 55.5, 54.8, 46.7, 40.6, 39.5, 33.5, 31.5, 28.5, 19.6, 17.0·; HRMS (ESI): *m*/*z* calcd for $C_{24}H_{29}F_3N_5O_4$ $[M + H]^+$ 508.2172 found 508.2169.

(*S*)-*N*-((*S*)-1-Cyano-2-((*S*)-2-oxopiperidin-3-yl)ethyl)-2-((2,2,2-trifluoroacetyl)-L-valyl)-1,2,3,4-tetrahydroisoquinoline-3-carboxamide (5f). Following the ester hydrolysis procedure described in general procedure **B**, the reaction of ester **15b** (40 mg, 0.10 mmol) afforded the acid (30 mg, 80% crude yield) as a white fluffy solid. Amine **7b** (22 mg, 0.08 mmol) was deprotected and coupled with the corresponding acid (32 mg, 0.08 mmol) using the same procedure **B** described above, affording compound **5f** as a white solid (17 mg, 42%). The analytical HPLC purity of compound **5f** was determined by using an HPLC-Agilent 1260 infinity (VYDAC, protein and peptide C18), 38% ACN/H_2O, 0.5 mL min^{-1}, t_r: 16.35 min, purity = 96%. ^1H NMR of major rotamer (400 MHz, $CDCl_3$) δ 8.52 (d, J = 6.0 Hz, 1H), 7.24–7.16 (m, 4H), 5.91 (s, 1H), 4.99 (dd, J = 8.9, 5.2 Hz, 1H), 4.78 (t, J = 6.6 Hz, 1H), 4.71 (d, J =

2.4 Hz, 1H), 4.65 (dt, J = 11.1, 5.2 Hz, 1H), 3.35–3.29 (m, 2H), 3.23–3.11 (m, 2H), 2.45–2.30 (m, 2H), 2.11–2.03 (m, 1H), 2.00–1.93 (m, 1H), 1.89–1.81 (m, 2H), 1.73–1.69 (m, 1H), 1.57–1.51 (m, 1H), 1.11 (d, J = 6.8 Hz, 3H), 0.96 (dd, J = 6.8, 4.1 Hz, 3H); ^{13}C NMR of major rotamer (126 MHz, $CDCl_3$) δ 175.1, 171.2, 170.3, 157.7–156.5 (m), 133.4, 132.8, 128.2, 127.8, 127.2, 126.1, 118.3, 117.0–114.7 (m), 55.5, 54.8, 46.7, 42.4, 39.4, 37.6, 34.3, 31.5, 27.4, 21.2, 19.7, 16.9; HRMS (ESI): m/z calcd for $C_{25}H_{31}F_3N_5O_4$ $[M + H]^+$ 522.2328 found 522.2312.

(*S*)-*N*-((*S*)-1-Cyano-2-((*S*)-2-oxopyrrolidin-3-yl)ethyl)-2-((*S*)-3,3-dimethyl-2-(2,2,2-trifluoroacetamido)butanoyl)-1,2,3,4-tetrahydroisoquinoline-1-carboxamide (5g). Following the ester hydrolysis procedure described in general procedure **B**, the reaction of ester **18** (40 mg, 0.10 mmol) afforded the acid (27 mg, 70% crude yield) as a white fluffy solid. Amine **7a** (18 mg, 0.07 mmol) was deprotected and coupled with the corresponding acid (27 mg, 0.07 mmol) using the same procedure **B** described above, affording compound **5g** as a white solid (15 mg, 42%). The analytical HPLC purity of compound **5g** was determined by using an HPLC-Agilent 1260 infinity (VYDAC, protein and peptide C18), 40% ACN/H_2O, 0.5 mL min^{-1}, t_r: 17.88 min, purity = 96%. ^{1}H NMR of major rotamer (400 MHz, $CDCl_3$) δ 8.51 (d, J = 6.0 Hz, 1H), 7.44–7.38 (m, 1H), 7.31–7.25 (m, 2H), 7.21–7.17 (m, 1H), 7.10–7.04 (d, J = 9.4 Hz, 1H), 5.83–5.73 (m, 2H), 5.00 (d, J = 9.3 Hz, 1H), 4.73 (td, J = 11.8, 6.3 Hz, 1H), 4.20–4.10 (m, 1H), 3.82–3.72 (m, 1H), 3.44–3.32 (m, 2H), 3.14 (td, J = 9.5, 4.2 Hz, 1H), 2.88 (dt, J = 15.9, 5.1 Hz, 1H), 2.62–2.51 (m, 1H), 2.48–2.38 (m, 1H), 2.35–2.24 (m, 1H), 2.02–1.88 (m, 1H), 1.51–1.41 (m, 1H), 1.10 (s, 9H); ^{13}C NMR of major rotamer (126 MHz, $CDCl_3$) δ 179.4, 170.6, 169.9, 157.3–156.3 (m), 135.1, 130.5, 128.5, 128.3, 127.4, 127.3, 118.2, 117.0–114.7 (m), 58.6, 55.6, 43.8, 40.6, 39.6, 36.8, 33.9, 28.8, 28.4, 26.4; HRMS (ESI): m/z calcd for $C_{25}H_{31}F_3N_5O_4$ $[M + H]^+$ 522.2328 found 522.2326.

***tert*-Butyl ((*S*)-1-((*S*)-3-(((*S*)-1-(benzo[*d*]thiazol-2-yl)-1-oxo-3-((S)-2-oxopyrrolidin-3-yl)propan-2-yl)carbamoyl)-3,4-dihydroisoquinolin-2(1*H*)-yl)-3,3-dimethyl-1-oxobutan-2-yl) carbamate (5h).** Following the general procedure **A**, the reaction of ester **14b** (25 mg, 0.06 mmol) afforded the acid (20 mg, 85% crude yield) as a white fluffy solid. Amine **12a** (20 mg, 0.05 mmol) was deprotected and coupled with the corresponding acid (20 mg, 0.07 mmol) using the same procedure **B** described above, affording compound **5h** as a white solid (18 mg, 54%). The analytical HPLC purity of compound **5h** was determined by using an HPLC-Agilent 1260 infinity (VYDAC, protein and peptide C18), 50% ACN/H_2O, 1.0 mL min^{-1}, t_r: 11.67 min, purity = 94%. ^{1}H NMR (500 MHz, $CDCl_3$) δ 8.14 (dd, J = 7.6, 1.5 Hz, 1H), 7.96 (dd, J = 7.6, 1.5 Hz, 1H), 7.60–7.49 (m, 3H), 7.22–7.17 (m, 3H), 7.16–7.11 (m, 1H), 5.98 (s, 1H), 5.82–5.74 (m, 1H), 5.33 (d, J = 9.8 Hz, 1H), 5.04–4.94 (m, 2H), 4.75–4.65 (m, 2H), 3.35–3.22 (m, 3H), 3.14–3.07 (m, 1H), 2.48–2.35 (m, 1H), 2.17–2.02 (m, 3H), 2.00–1.87 (m, 1H), 1.40 (s, 9H), 1.12 (s, 9H); ^{13}C NMR of major rotamer (126 MHz, $CDCl_3$) δ 192.3, 179.7, 172.5, 171.1, 163.6, 155.6, 153.4, 137.3, 134.1, 133.4, 128.0, 127.8, 127.1, 127.0, 125.7, 122.4, 79.6, 56.7, 55.2, 54.0, 47.5, 40.4, 38.1, 36.2, 34.1, 31.9, 28.4, 26.7, 26.5; HRMS (ESI): m/z calcd for $C_{35}H_{44}N_5O_6S$ $[M + H]^+$ 662.3012 found 662.3000.

(*S*)-*N*-((*S*)-1-(Benzo[*d*]thiazol-2-yl)-1-oxo-3-((S)-2-oxopyrrolidin-3-yl)propan-2-yl)-2-((*S*)-3,3-dimethyl-2-(2,2,2-trifluoroacetamido) butanoyl)-1,2,3,4-tetrahydroisoquinoline-3-carboxamide (5i). Following the ester hydrolysis procedure described in general procedure **B**, the reaction of ester **15a** (28 mg, 0.07 mmol) afforded the acid (19 mg, 70% crude yield) as a white fluffy solid. Amine **12a** (20 mg, 0.05 mmol) was deprotected and coupled with the corresponding acid (19 mg, 0.05 mmol) using the same procedure **B** described above, affording compound **5i** as a white solid (17 mg, 52%). The analytical HPLC purity of compound **5i** was determined by using an HPLC-Agilent 1260 infinity (VYDAC, protein and peptide C18), 47% ACN/H_2O, 0.5 mL min^{-1}, t_r: 33.30 min, purity = 95%. ^{1}H NMR of major rotamer (500 MHz, $CDCl_3$) δ 8.19–8.13 (m, 1H), 7.99–7.92 (m, 1H), 7.61–7.48 (m, 3H), 7.24–7.18 (m, 3H), 7.17–7.14 (m, 1H), 6.30–6.21 (m, 1H), 5.87–5.72 (m, 1H), 5.10–5.01 (m, 1H), 4.92–4.83 (m, 2H), 4.73–4.65 (m, 1H), 3.36–3.27 (m, 2H), 3.25–3.19 (m, 2H), 2.58–2.33 (m, 2H), 2.29–2.07 (m, 2H), 2.04–1.97 (m, 1H), 1.13 (s, 9H); ^{13}C NMR of major rotamer (126 MHz, $CDCl_3$) δ 192.3, 180.4, 171.1, 169.8, 169.4, 163.9, 157.1–156.7 (m), 153.4, 137.3, 133.9, 133.3, 128.2, 128.1, 127.6, 127.2, 125.9, 125.7, 122.5, 117.0–114.7 (m), 56.1, 55.9, 47.9, 44.5, 40.7, 38.6, 37.2, 33.8, 31.9, 26.5; HRMS (ESI): m/z calcd for $C_{32}H_{35}F_3N_5O_5S$ $[M + H]^+$ 658.2311 found 658.2295.

(*S*)-*N*-((*S*)-1-(Benzo[*d*]thiazol-2-yl)-1-oxo-3-((*S*)-2-oxopiperidin-3-yl)propan-2-yl)-2-((*S*)-3,3-dimethyl-2-(2,2,2-trifluoroacetamido) butanoyl)-1,2,3,4-tetrahydroisoquinoline-3-carboxamide (5j). Following the ester hydrolysis procedure described in general procedure **B**, the reaction of ester **15a** (28 mg, 0.07 mmol) afforded acid (19 mg, 70% crude yield) as a white fluffy solid. Amine **12b** (20 mg, 0.05 mmol) was deprotected and coupled with the corresponding acid (19 mg, 0.05 mmol) using the same procedure **B** described above, affording compound **5j** as a white solid (15 mg, 48%). The analytical HPLC purity of compound **5j** was determined by using an HPLC-Agilent 1260 infinity (VYDAC, protein and peptide C18), 50% ACN/H_2O, 1.0 mL min^{-1}, t_r: 11.52 min, purity = 95%; ^{1}H NMR (500 MHz, $CDCl_3$) δ 8.18–8.12 (m, 1H), 7.99–7.95 (m, 1H), 7.92–7.84 (m, 1H), 7.61–7.47 (m, 2H), 7.24–7.13 (m, 5H), 5.87 (s, 1H), 5.80–5.69 (m, 1H), 5.11–4.95 (m, 1H), 4.96–4.81 (m, 2H), 4.72–4.57 (m, 1H), 3.37–3.24 (m, 2H), 3.24–3.17 (m, 2H), 2.40–2.29 (m, 1H), 2.26–2.18 (m, 1H), 2.10–1.86 (m, 2H), 1.82–1.61 (m, 3H), 1.08 (s, 9H); ^{13}C NMR of major rotamer (126 MHz, $CDCl_3$) δ 192.4, 170.9, 169.7, 164.0, 156.9–156.6 (m), 153.5, 137.3, 133.8, 133.2, 128.1, 127.9, 127.8, 127.2, 127.1, 127.0, 125.9, 125.6, 122.4, 117.0–114.7 (m), 55.9, 55.7, 54.5, 47.7, 44.4, 42.4, 38.6, 37.2, 34.0, 31.8, 26.5, 21.7; HRMS (ESI): m/z calcd for $C_{33}H_{37}F_3N_5O_5S$ $[M + H]^+$ 672.2467 found 672.2455.

(*S*)-*N*-((*S*)-1-(Benzo[*d*]thiazol-2-yl)-1-oxo-3-((*S*)-2-oxopyrrolidin-3-yl)propan-2-yl)-2-((*S*)-3,3-dimethyl-2-(2,2,2-trifluoroacetamido) butanoyl)-1,2,3,4-tetrahydroisoquinoline-1-carboxamide (5k). Following the ester hydrolysis procedure described in general

procedure **B**, the reaction of ester **18** (28 mg, 0.07 mmol) afforded the acid (19 mg, 70% crude yield) as a white fluffy solid. Amine **12a** (20 mg, 0.05 mmol) was deprotected and coupled with the corresponding acid (19 mg, 0.05 mmol) using the same procedure **B** described above, affording compound **5k** as a white solid (16 mg, 48%). The analytical HPLC purity of compound **5k** was determined by using an HPLC-Agilent 1260 infinity (VYDAC, protein and peptide C18), 45% ACN/H_2O, 0.7 mL min^{-1}, t_r: 23.33 min, purity = 94%. ^1H NMR of major rotamer (400 MHz, $CDCl_3$) δ 8.13 (d, J = 8.2 Hz, 1H), 7.96 (d, J = 8.2 Hz, 1H), 7.88 (d, J = 6.8 Hz, 1H), 7.61–7.49 (m, 3H), 7.46–7.39 (m, 1H), 7.24–7.20 (m, 2H), 7.17–7.10 (m, 2H), 5.98 (s, 1H), 5.76–5.67 (m, 1H), 5.64–5.59 (m, 1H), 5.01 (d, J = 9.1 Hz, 1H), 4.10–4.00 (m, 1H), 3.92–3.82 (m, 1H), 3.43–3.31 (m, 2H), 3.09–3.00 (m, 1H), 2.93–2.81 (m, 1H), 2.67–2.58 (m, 1H), 2.23–2.14 (m, 1H), 2.09–1.97 (m, 1H), 1.10 (s, 9H); ^{13}C NMR of major rotamer (126 MHz, $CDCl_3$) δ 192.0, 170.2, 169.6, 169.1, 157.0–156.7 (m), 153.4, 134.8, 131.0, 128.5, 128.1, 128.0, 127.9, 127.6, 127.1, 125.7, 122.4, 117.0–114.7 (m), 58.2, 55.5, 55.0, 43.6, 40.5, 37.0, 33.8, 28.9, 28.5, 26.5; HRMS (ESI): m/z calcd for $C_{32}H_{35}F_3N_5O_5S$ $[M + H]^+$ 658.2311 found 658.2295.

***tert*-Butyl ((*S*)-3,3-dimethyl-1-oxo-1-((*S*)-3-(((*S*)-1-oxo-3-((*S*)-2-oxopyrrolidin-3-yl)-1-(4-phenylthiazol-2-yl)propan-2-yl) carbamoyl)-3,4-dihydroisoquinolin-2(1*H*)-yl)butan-2-yl) carbamate (5l).** Following the ester hydrolysis procedure described in general procedure **B**, the reaction of ester **14b** (25 mg, 0.06 mmol) afforded the acid (19 mg, 80% crude yield) as a white fluffy solid. Amine **13a** (21 mg, 0.05 mmol) was deprotected and coupled with the corresponding acid (19 mg, 0.05 mmol) using the same procedure **B** described above, affording compound **5l** as a white solid (19 mg, 55%). The analytical HPLC purity of compound **5l** was determined by using an HPLC-Agilent 1260 infinity (VYDAC, protein and peptide C18), 45% ACN/H_2O, 0.5 mL min^{-1}, t_r: 58.23 min, purity = 92%; ^1H NMR (400 MHz, DMSO) δ 8.69–8.59 (m, 2H), 8.05–7.98 (m, 2H), 7.63 (s, 1H), 7.52–7.44 (m, 2H), 7.43–7.34 (m, 1H), 7.22–7.06 (m, 4H), 6.70–6.53 (m, 1H), 5.63–5.40 (m, 1H), 4.90–4.81 (m, 1H), 4.63–4.45 (m, 2H), 3.23–2.97 (m, 4H), 2.92–2.57 (m, 1H), 2.37–2.22 (m, 1H), 2.10–1.96 (m, 1H), 1.89–1.68 (m, 2H), 1.34 (s, 9H), 0.98 (s, 9H); ^{13}C NMR of major rotamer (126 MHz, DMSO) δ 191.8, 178.6, 171.9, 171.0, 164.4, 156.9, 135.6. 129.5, 129.3, 127.8, 127.5, 126.9, 126.7, 126.1, 122.9, 78.6, 55.0, 53.2, 46.9, 38.1, 35.8, 33.6, 31.9, 28.7, 28.0, 26.8, 26.8; HRMS (ESI): m/z calcd for $C_{37}H_{46}N_5O_6S$ $[M + H]^+$ 688.3169 found 688.3163.

(*S*)-2-((*S*)-3,3-Dimethyl-2-(2,2,2-trifluoroacetamido)butanoyl)-*N*-((*S*)-1-oxo-3-((*S*)-2-oxopyrrolidin-3-yl)-1-(4-phenylthiazol-2-yl) propan-2-yl)-1,2,3,4-tetrahydroisoquinoline-3-carboxamide (5m). Following the ester hydrolysis procedure described in general procedure **B**, the reaction of ester **15a** (28 mg, 0.07 mmol) afforded the acid (19 mg, 70% crude yield) as a white fluffy solid. Amine **13a** (21 mg, 0.05 mmol) was deprotected and coupled with the corresponding acid (19 mg, 0.05 mmol) using the same procedure **B** described above, affording compound **5m** as a white solid (16 mg, 48%). The analytical HPLC purity of compound **5m** was determined by using an HPLC-Agilent 1260 infinity (VYDAC, protein and peptide C18), 50% ACN/H_2O, 0.5 mL min^{-1}, t_r: 23.91 min, purity = 95%. ^1H NMR (400 MHz, $CDCl_3$) δ 7.91–7.88 (s, 2H), 7.85 (s, 1H), 7.48–7.42 (m, 4H), 7.41–7.36 (td, J = 7.1, 1.5 Hz, 1H), 7.23–7.21 (m, 2H), 7.18–7.16 (m, 2H), 5.77 (t, J = 8.0 Hz, 1H), 5.06 (d, J = 9.2 Hz, 1H), 4.86–4.80 (m, 2H), 4.68 (d, J = 14.7 Hz, 1H), 3.39–3.25 (m, 3H), 3.23–3.17 (m, 2H), 2.61–2.42 (m, 1H), 2.22–2.14 (m, 1H), 2.14–1.80 (m, 3H), 1.14 (s, 9H); ^{13}C NMR of major rotamer (126 MHz, $CDCl_3$) δ 190.6, 179.8, 170.8, 169.8, 163.6, 157.7–156.9 (m), 133.8, 133.3, 133.1, 129.0, 128.1, 127.7, 127.3, 126.4, 120.6, 115.2–110.7 (m), 55.9, 55.9, 54.2, 47.7, 40.6, 38.5, 38.3, 37.1, 34.3, 31.8, 26.5; HRMS (ESI): m/z calcd for $C_{34}H_{37}F_3N_5O_5S$ $[M + H]^+$ 684.2467 found 684.2455.

(*S*)-2-((*S*)-3,3-Dimethyl-2-(2,2,2-trifluoroacetamido)butanoyl)-*N*-((*S*)-1-oxo-3-((*S*)-2-oxopiperidin-3-yl)-1-(4-phenylthiazol-2-yl) propan-2-yl)-1,2,3,4-tetrahydroisoquinoline-3-carboxamide (5n). Following the ester hydrolysis procedure described in general procedure **B**, the reaction of ester **15a** (28 mg, 0.07 mmol) afforded the acid (19 mg, 70% crude yield) as a white fluffy solid. Amine **13b** (22 mg, 0.05 mmol) was deprotected and coupled with the corresponding acid (19 mg, 0.05 mmol) using the same procedure **B** described above, affording compound **5n** as a white solid (18 mg, 50%). The analytical HPLC purity of compound **5n** was determined by using an HPLC-Agilent 1260 infinity (VYDAC, protein and peptide C18), 47% ACN/H_2O, 0.5 mL min^{-1}, t_r: 43.66 min, purity = 99%. ^1H NMR of major rotamer (400 MHz, $CDCl_3$) δ 7.93–7.87 (m, 2H), 7.84 (s, 1H), 7.46–7.43 (m, 2H), 7.41–7.37 (m, 1H), 7.23–7.20 (m, 3H), 7.19–7.14 (m, 2H), 5.92–5.82 (m, 1H), 5.77–5.67 (m, 1H), 5.10–5.02 (m, 1H), 4.89–4.81 (m, 2H), 4.72–4.66 (m, 1H), 3.36–3.24 (m, 2H), 3.23–3.18 (m, 2H), 2.35–2.21 (m, 3H), 2.16–2.07 (m, 1H), 2.04–1.92 (m, 1H), 1.68–1.51 (m, 2H), 1.14 (s, 9H); ^{13}C NMR of major rotamer (126 MHz, $CDCl_3$) δ 190.9, 170.9, 169.8, 164.0, 157.6, 157.4–156.9 (m), 133.8, 133.5, 133.2, 129.0, 128.9, 128.1, 127.8, 127.1, 126.4, 125.9, 120.3, 117.0–114.7 (m), 56.0, 55.7, 54.2, 47.8, 44.8, 42.4, 37.2, 34.3, 31.8, 27.1, 26.5, 21.6; HRMS (ESI): m/z calcd for $C_{35}H_{39}F_3N_5O_5S$ $[M + H]^+$ 698.2624 found 698.2615.

(*S*)-*N*-((*S*)-1-Cyano-2-((*S*)-2-oxopiperidin-3-yl)ethyl)-2-((4-methoxy-1*H*-indole-2-carbonyl)-L-leucyl)-1,2,3,4-tetrahydroisoquinoline-3-carboxamide (5o). Following the ester hydrolysis procedure described in general procedure **B**, the reaction of ester **20** (45 mg, 0.09 mmol) afforded the acid (34 mg, 79% crude yield) as a white fluffy solid. Amine **7b** (20 mg, 0.07 mmol) was deprotected and coupled with the corresponding acid (34 mg, 0.07 mmol) using the same procedure **B** described above, affording compound **5o** as a white solid (19 mg, 42%). The analytical HPLC purity of compound **5o** was determined by using an HPLC-Agilent 1260 infinity (VYDAC, protein and peptide C18), 40% ACN/H_2O, 0.5 mL min^{-1}, t_r 30.26 min, purity = 95%. ^1H NMR of major rotamer (500 MHz, $CDCl_3$) δ 10.68 (s, 1H), 9.48 (d, J = 6.7 Hz, 1H), 7.27–7.20 (m, 1H), 7.18–7.13 (m, 3H), 7.12–7.08 (m, 1H), 7.07–7.02 (m, 1H), 6.92 (d, J = 6.5 Hz, 1H), 6.48 (d, J = 7.4 Hz, 1H), 5.92 (s, 1H), 5.24 (d, J = 17.4 Hz, 1H), 5.08–5.03 (m, 1H), 4.94–4.86 (m, 1H), 4.53 (ddd, J = 11.7, 6.7, 4.5 Hz, 1H), 4.13 (d, J = 17.4 Hz, 1H),

3.94 (s, 3H), 3.69–3.62 (m, 1H), 3.28–3.20 (m, 2H), 3.05–2.95 (m, 2H), 2.33 (dq, J = 10.3, 6.4 Hz, 1H), 1.91–1.84 (m, 2H), 1.83–1.72 (m, 4H), 1.63–1.52 (m, 2H), 1.16–1.06 (m, 1H), 1.08–0.92 (m, 6H); ^{13}C NMR of major rotamer (126 MHz, $CDCl_3$) δ 173.4, 172.2, 169.5, 163.1, 154.2, 138.7, 132.1, 131.0, 128.7, 128.0, 127.2, 126.7, 126.2, 125.6, 118.8, 118.7, 105.7, 101.3, 99.4, 55.7, 55.3, 48.9, 42.9, 42.2, 40.8, 38.7, 37.0, 33.0, 30.3, 25.2, 25.0, 23.2, 22.1, 21.2; HRMS (ESI): m/z calcd for $C_{34}H_{41}N_6O_5$ $[M + H]^+$ 613.3138 found 613.3128.

(*S*)-2-((4-Methoxy-1*H*-indole-2-carbonyl)-L-leucyl)-*N*-((*S*)-1-oxo-3-((*S*)-2-oxopyrrolidin-3-yl)-1-(4-phenylthiazol-2-yl)propan-2-yl)-1,2,3,4-tetrahydroisoquinoline-3-carboxamide (5p). Following the ester hydrolysis procedure described in general procedure **B**, the reaction of ester **20** (45 mg, 0.09 mmol) afforded the acid (34 mg, 79% crude yield) as a white fluffy solid. Amine **13a** (29 mg, 0.07 mmol) was deprotected and coupled with the corresponding acid (34 mg, 0.07 mmol) using the same procedure **B** described above, affording compound **5p** as a white solid (24 mg, 46%). The analytical HPLC purity of compound **5p** was determined by using an HPLC-Agilent 1260 infinity (VYDAC, protein and peptide C18), 50% ACN/H_2O, 0.5 mL min^{-1}, t_r: 29.88 min, purity = 94%. ^{1}H NMR (500 MHz, $CDCl_3$) δ 11.05 (d, J = 2.4 Hz, 1H), 9.52 (d, J = 6.0 Hz, 1H), 7.87–7.81 (m, 2H), 7.74 (s, 1H), 7.43–7.32 (m, 3H), 7.18–7.13 (m, 3H), 7.13–7.11 (m, 1H), 7.11–7.09 (m, 2H), 6.92 (d, J = 5.8 Hz, 1H), 6.44 (dd, J = 6.8, 1.6 Hz, 1H), 6.06 (s, 1H), 5.49–5.37 (m, 1H), 5.30 (d, J = 17.4 Hz, 1H), 5.09 (dd, J = 5.6, 2.1 Hz, 1H), 5.06–4.97 (m, 1H), 4.30 (d, J = 17.4 Hz, 1H), 3.94 (s, 3H), 3.63 (dd, J = 15.9, 1.9 Hz, 1H), 3.40–3.29 (m, 2H), 3.00 (dd, J = 15.9, 5.6 Hz, 1H), 2.81–2.68 (m, 1H), 2.35 (ddd, J = 12.9, 6.7, 2.4 Hz, 1H), 2.18–1.99 (m, 3H), 1.92–1.77 (m, 3H), 1.62–1.52 (m, 1H), 1.04–1.00 (m, 6H); ^{13}C NMR of major rotamer (126 MHz, $CDCl_3$) δ 190.8, 180.3, 172.3, 170.0, 164.2, 163.1, 157.4, 154.1, 138.8, 133.6, 132.4, 131.3, 128.9, 128.8, 128.6, 128.1, 127.0, 126.6, 126.4, 126.3, 125.3, 120.1, 118.8, 105.9, 101.0, 99.2, 55.6, 55.5, 55.3, 49.4, 42.8, 40.7, 40.3, 38.3, 32.0, 30.1, 26.6, 25.1, 23.4, 22.0; HRMS (ESI): m/z calcd for $C_{42}H_{45}N_6O_6S$ $[M + H]^+$ 761.3121 found 761.3116.

(*S*)-2-((4-Methoxy-1*H*-indole-2-carbonyl)-L-leucyl)-*N*-((S)-1-oxo-3-((*S*)-2-oxopiperidin-3-yl)-1-(4-phenylthiazol-2-yl)propan-2-yl)-1,2,3,4-tetrahydroisoquinoline-3-carboxamide (5q). Following the ester hydrolysis procedure described in general procedure **B**, the reaction of ester **20** (45 mg, 0.09 mmol) afforded the acid (34 mg, 79% crude yield) as a white fluffy solid. Amine **13b** (30 mg, 0.07 mmol) was deprotected and coupled with the corresponding acid (34 mg, 0.07 mmol) using the same procedure **B** described above, affording compound **5q** as a white solid (24 mg, 44%). The analytical HPLC purity of compound **5q** was determined by using an HPLC-Agilent 1260 infinity (VYDAC, protein and peptide C18), 50% ACN/H_2O, 0.5 mL min^{-1}, t_r: 39.35 min, purity = 94%. ^{1}H NMR (400 MHz, $CDCl_3$) δ 11.19 (s, 1H), 9.56 (d, J = 6.2 Hz, 1H), 7.91–7.82 (m, 2H), 7.75 (s, 1H), 7.43–7.34 (m, 3H), 7.19–7.14 (m, 3H), 7.11–7.06 (m, 3H), 6.80 (d, J = 5.8 Hz, 1H), 6.48–6.38 (m, 1H), 6.02 (s, 1H), 5.57–5.45 (m, 1H), 5.27 (d, J = 17.3 Hz, 1H), 5.13–4.98 (m, 2H), 4.27 (d, J = 17.3 Hz, 1H), 3.93 (s, 3H), 3.63 (d, J = 15.7 Hz, 1H), 3.39–3.31 (m, 2H), 2.99 (dd, J = 15.8, 5.5 Hz, 1H), 2.86 (td, J = 13.4, 3.4 Hz, 2H), 2.21–2.09 (m, 1H), 2.04–1.92 (m, 2H), 1.91–1.78 (m, 3H), 1.77–1.63 (m, 2H), 1.63–1.54 (m, 1H), 1.06–0.99 (m, 6H); ^{13}C NMR of major rotamer (101 MHz, $CDCl_3$) δ 191.2, 174.7, 172.2, 170.0, 164.1, 163.0, 157.2, 154.0, 138.6, 133.5, 132.5, 131.3, 128.7, 128.6, 128.2, 126.9, 126.4, 126.3, 126.1, 125.0, 119.9, 118.7, 105.8, 100.7, 99.0, 55.6, 55.1, 54.0, 49.3, 42.8, 42.3, 40.5, 37.6, 31.5, 30.2, 25.0, 24.4, 23.3, 21.9, 20.6; HRMS (ESI): m/z calcd for $C_{43}H_{47}N_6O_6S$ $[M + H]^+$ 775.3278 found 775.3272.

X-ray structure determination of inhibitors 5c, 5j, 5m-bound to SARS-CoV-2 3CLpro

Co-crystals of SARS-CoV-2 3CLpro with **5c** (GRL-05122), **5j** (GRL-06222), and **5m** (GRL-05022) were grown at 4 °C using the sitting-drop or hanging-drop vapor diffusion method as described previously.[27,53] Briefly, 1 μL of ~110 μM SARS-CoV-2 3CLpro in 25 mM HEPES pH 7.5 and 2.5 mM DTT containing ~150 μM inhibitors **5c**, **5j**, and **5m** were separately mixed with 2 μL of reservoir solution which contained a constant concentration of 3 mM DTT, 50 mM MES pH 6.0, 1% MPD, and varying concentrations of PEG-10000 and KCl. Crystals that formed were removed using nylon loops and transferred into 3 μL of a cryo-solution containing the crystallization solution and inhibitor that was supplemented with 30% MPD. Crystals were soaked in the resulting solution for about 30 minutes and then flash-frozen in liquid nitrogen for X-ray data collection.

X-ray diffraction data were collected on crystals using Life Sciences Collaborative Access Team (LS-CAT) beamline 21-ID-F at the Advanced Photon Source, Argonne National Laboratory. X-ray data were indexed, integrated and scaled using the HKL2000 software package.[54] The software package PHENIX was used for structure determination *via* molecular replacement and iterative rounds of structural refinement.[55] Inhibitor coordinates and restraints were generated using eLBOW (PHENIX).[56] Manual modeling building was performed using Coot.[57] Automated structural refinement was performed using the refine module available in PHENIX. The X-ray data collection and refinement statistics for the SARS-CoV-2 Mpro with inhibitor **5c** (GRL-05122), **5j** (GRL-06222), and **5m** (GRL-05022) complexes are summarized in Table S1.[58] The resulting coordinates and associated reflection files are deposited in the PDB under accession numbers: 9E7S, 9ZO3, 9ZNL.

Determination of antiviral activity

VeroE6 cells and TMPRSS2-overexpressing VeroE6 (VeroE6TMPRSS2) cells were obtained from the Japanese Collection of Research Bioresources (JCRB) Cell Bank (Osaka, Japan). VeroE6 cells were maintained in Dulbecco's modified Eagle's medium (d-MEM) supplemented with 10% fetal bovine serum (FCS), 100 μg mL^{-1} of penicillin, and 100 μg mL^{-1} of streptomycin. VeroE6TMPRSS2 cells were maintained in d-MEM as reported[27] in the presence of 1 mg mL^{-1} of

G418. SARS-CoV-2 strain JPN/TY/WK-521 (SARS-CoV-2WK-521) was obtained from the National Institute of Infectious Diseases (Tokyo, Japan). Antiviral assay was carried out as described by us previously.[27]

Conflicts of interest

There are no conflicts to declare.

Abbreviations used

DIPEA	Diisopropylethylamine
MPro	Main protease
PDB	Protein data base
SAR	Structure–activity relationship
SARS-CoV-2	Severe acute respiratory syndrome Coronavirus-2
THIQ	Tetrahydroisoquinoline
TFAA	Trifluoroacetic anhydride

Data availability

X-ray crystallographic data of compounds **5c**, **5j**, **5m**-bound to SARS-CoV-2 3CLpro has been deposited at the PDB (9E7S, 9ZO3, 9ZNL). Spectral data, assay, and X-ray data supporting this article are available for public use. SI for this article can be found online, including full NMR spectroscopic data for all final compounds, methods for expression and purification of SARS-CoV-2 Mpro, methods for SARS-CoV-2 Mpro inhibition assay, methods for crystallization of SARS-CoV Mpro with inhibitors, and X-ray structural data for inhibitors-bound SARS-CoV-2 MPro. See DOI: https://doi.org/10.1039/d6md00312e.

Acknowledgements

The research reported here was supported in part by grants and a contract from the National Institute of Allergy and Infectious Diseases, National Institutes of Health (A. K. G. AI150466, and A. K. G. & A. D. M., AI158649 and contract HHSN272201700060C). The present work was also supported by a grant for Development of Novel Drugs for Treating COVID-19 from the Intramural Research Program of National Center for Global Health and Medicine (H. M., 19A3001 and Y. T., 22A2008D), in part by Japan Agency for Medical Research and Development (AMED) (H. M., 21fk0108480). UJ was supported by NIH NIAID T32 training grant AI 148103 (Drug Discovery in Infectious Disease Training) and SB was supported by NIH NIGMS T32 training grant GM132024 (Purdue University Molecular Biophysics Training Program). The authors also wish to acknowledge support from the Purdue Institute for Cancer Research, NIH grant P30 CA023168, for use of the shared NMR and Macromolecular Crystallization and X-ray diffraction facilities available in the Biomolecular Structure Shared Resource. In-house X-ray data were recorded on a Rigaku MicroMax-007 HF rotating anode generator coupled to a Dectris Eiger2 hybrid photon counting detector as supported by NIH S10 grant OD030507. X-ray data were also collected at the Life Sciences Collaborative Access Team (LS-CAT) beamline 21-ID-F at the Advanced Photon Source (APS), Argonne National Laboratory (ANL). The APS is a U.S. Department of Energy (DOE) Office of Science User Facility operated for the DOE Office of Science by Argonne National Laboratory under Contract No. DE-AC02-06CH11357. Use of the LS-CAT Sector 21 was supported by the Michigan Economic Development Corporation and the Michigan Technology Tri-Corridor (Grant 085P1000817).

References

1 C. J. L. Murray, *Lancet*, 2022, **399**, 417–419.
2 H. Rutter, M. Wolpert and T. Greenhalgh, *Br. Med. J.*, 2020, **370**, m3349.
3 WHO Coronavirus (COVID-19) Dashboard, https://covid19.who.int, 2023, (accessed 2023-10-08).
4 C. Del Rio and P. N. Malani, *JAMA*, 2022, **327**, 2389–2390.
5 S. Pelly and D. Liotta, *ACS Cent. Sci.*, 2021, **7**, 396–399.
6 L.-L. Chen, S. M. U. Abdullah, W.-M. Chan, B. P.-C. Chan, J. D. Ip, A. W.-H. Chu, L. Lu, X. Zhang, Y. Zhao, V. W.-M. Chuang, A. K.-W. Au, V. C.-C. Cheng, S. Sridhar, K.-Y. Yuen, I. F.-N. Hung, K.-H. Chan and K. K.-W. To, *Nat. Commun.*, 2022, **13**, 3618.
7 L. Lu, B. W. Y. Mok, L. L. Chen, J. M. C. Chan, O. T. Y. Tsang, B. H. S. Lam, V. W. M. Chuang, A. W. H. Chu, W. M. Chan, J. D. Ip, B. P. C. Chan, R. Zhang, C. C. Y. Yip, V. C. C. Cheng, K. H. Chan, D. Y. Jin, I. F. N. Hung, K. Y. Yuen, H. Chen and K. K. W. To, *Clin. Infect. Dis.*, 2022, **75**, e822–e826.
8 S. S. A. Karim and Q. A. Karim, *Lancet*, 2021, **398**, 2126–2128.
9 A. K. Ghosh, M. Brindisi, D. Shahabi, M. E. Chapman and A. D. Mesecar, *ChemMedChem*, 2020, **15**, 907–932.
10 G. Li, R. Hilgenfeld, R. Whitley and E. De Clercq, *Nat. Rev. Drug Discovery*, 2023, **22**, 449–475.
11 L. Braconi, A. Sosic and L. Crocetti, *Bioorg. Med. Chem.*, 2025, **128**, 118247.
12 P. V. Baranov, C. M. Henderson, C. B. Anderson, R. F. Gesteland, J. F. Atkins and M. T. Howard, *Virology*, 2005, **332**, 498–510.
13 A. E. Gorbalenya, E. J. Snijder and J. Ziebuhr, *J. Gen. Virol.*, 2000, **81**, 853–879.
14 Y. M. Báez-Santos, S. E. St John and A. D. Mesecar, *Antiviral Res.*, 2015, **115**, 21–38.
15 X. Xu, *Nucleic Acids Res.*, 2003, **31**, 7117–7130.
16 K. Anand, J. Ziebuhr, P. Wadhwani, J. R. Mesters and R. Hilgenfeld, *Science*, 2003, **300**, 1763–1767.
17 V. Thiel, K. A. Ivanov, A. Putics, T. Hertzig, B. Schelle, S. Bayer, B. Weißbrich, E. J. Snijder, H. Rabenau, H. W. Doerr and A. E. Gorbalenya, *J. Gen. Virol.*, 2003, **84**, 2305–2315.
18 L. Zhang, D. Lin, X. Sun, U. Curth, C. Drosten, L. Sauerhering, S. Becker, K. Rox and R. Hilgenfeld, *Science*, 2020, **368**, 409–412.
19 K. Anand, G. J. Palm, J. R. Mesters, S. G. Siddell, J. Ziebuhr and R. Hilgenfeld, *EMBO J.*, 2002, **21**, 3213–3224.

20 D. A. Matthews, A. K. Patick, R. O. Baker, M. A. Brothers, P. S. Dragovich, C. J. Hartmann, T. O. Johnson, E. M. Mucker, S. H. Reich, P. A. J. Rejto, P. W. Rose, S. H. Zwiers and J. W. Huggins, *Learning from SARS: Preparing for the Next Disease Outbreak: Workshop Summary*, The National Academies Press, 2004, vol. 4, pp. 186–193.
21 A. K. Ghosh, K. Xi, M. E. Johnson, S. C. Baker and A. D. Mesecar, *Annu. Rep. Med. Chem.*, 2006, **41**, 183–196.
22 A. K. Ghosh, K. Xi, K. Ratia, B. D. Santarsiero, W. Fu, B. H. Harcourt, P. A. Rota, S. C. Baker, M. E. Johnson and A. D. Mesecar, *J. Med. Chem.*, 2005, **48**, 6767–6771.
23 A. K. Ghosh, J. L. Mishevich, A. D. Mesecar and H. Mitsuya, *ChemMedChem*, 2022, **17**, e202200440.
24 X. Pang, W. Xu, Y. Liu, H. Li and L. Chen, *Eur. J. Med. Chem.*, 2023, **257**, 115491.
25 A. K. Ghosh, G. Gong, V. Grum-Tokars, D. C. Mulhearn, S. C. Baker, M. Coughlin, B. S. Prabhakar, K. Sleeman, M. E. Johnson and A. D. Mesecar, *Bioorg. Med. Chem. Lett.*, 2008, **18**, 5684–5688.
26 P. Thanigaimalai, S. Konno, T. Yamamoto, Y. Koiwai, A. Taguchi, K. Takayama, F. Yakushiji, K. Akaji, S. E. Chen, A. Naser-Tavakolian and A. Schön, *Eur. J. Med. Chem.*, 2013, **68**, 372–384.
27 S. I. Hattori, N. Higashi-Kuwata, H. Hayashi, S. R. Allu, J. Raghavaiah, H. Bulut, D. Das, B. J. Anson, E. K. Lendy, Y. Takamatsu, N. Takamune, N. Kishimoto, K. Murayama, K. Hasegawa, M. Li, D. A. Davis, E. N. Kodama, R. Yarchoan, A. Wlodawer, S. Misumi, A. D. Mesecar, A. K. Ghosh and H. Mitsuya, *Nat. Commun.*, 2021, **12**, 668.
28 D. Focosi, S. McConnell, S. Shoham, A. Casadevall, F. Maggi and G. Antonelli, *Int. J. Antimicrob. Agents*, 2023, **61**, 106708.
29 Y. N. Lamb, *Drugs*, 2022, **82**, 585–591.
30 D. W. Kneller, H. Li, G. Phillips, K. L. Weiss, Q. Zhang, M. A. Arnould, C. B. Jonsson, S. Surendranathan, J. Parvathareddy, M. P. Blakeley and L. Coates, *Nat. Commun.*, 2022, **13**, 2268.
31 Y. R. Alugubelli, Z. Z. Geng, K. S. Yang, N. Shaabani, K. Khatua, X. R. Ma, E. C. Vatansever, C. C. Cho, Y. Ma, J. Xiao and L. R. Blankenship, *Eur. J. Med. Chem.*, 2022, **240**, 114596.
32 C. Marzolini, D. R. Kuritzkes, F. Marra, A. Boyle, S. Gibbons, C. Flexner, A. Pozniak, M. Boffito, L. Waters, D. Burger, D. J. Back and S. Khoo, *Clin. Pharmacol. Ther.*, 2022, **211**, 1191–1200.
33 NIH, *COVID-19 Treatment Guidelines*, 2023, (accessed 2023-10-08).
34 E. Mahase, *Br. Med. J.*, 2021, **375**, n2713.
35 J. Liu, X. Pan, S. Zhang, M. Li, K. Ma, C. Fan, Y. Lv, X. Guan, Y. Yang, X. Ye, X. Deng, Y. Wang, L. Qin, Z. Xia, Z. Ge, Q. Zhou, X. Zhang, Y. Ling, T. Qi, Z. Wen, S. Huang, L. Zhang, T. Wang, Y. Liu, Y. Huang, W. Li, H. Du, Y. Chen, Y. Xu, Q. Zhao, R. Zhao, D. Annane, J. Qu and D. Chen, *Lancet*, 2023, **33**, 100694.
36 C. Marzolini, D. R. Kuritzkes, F. Marra, A. Boyle, S. Gibbons, C. Flexner, A. Pozniak, M. Boffito, L. Waters, D. Burger, D. Back and S. Khoo, *Ann. Intern. Med.*, 2022, **175**, 744–746.
37 N. Niraj, S. S. Mahajan, A. Prakash, P. Sarma and B. Medhi, *Indian J. Pharmacol.*, 2022, **54**, 452–458.
38 A. Zagórska, A. Czopek, M. Fryc and J. Jończyk, *Biomolecules*, 2024, **14**, 797.
39 C. M. Allerton, J. T. Arcari, L. M. Aschenbrenner, M. Avery, B. M. Bechle, M. A. Behzadi, B. Boras, L. M. Buzon, R. D. Cardin, N. R. Catlin and A. A. Carlo, *J. Med. Chem.*, 2024, **67**, 13550–13571.
40 S. E. Greasley, S. Noell, O. Plotnikova, R. Ferre, W. Liu, B. Bolanos, K. Fennell, J. Nicki, T. Craig, Y. Zhu and A. E. Stewart, *J. Biol. Chem.*, 2022, **298**, 6.
41 B. K. Kumar, K. V. G. C. Sekhar, S. Chander, S. Kunjiappan and S. Murugesan, *RSC Adv.*, 2021, **11**, 12254–12287.
42 Faheem, B. K. Kumar, K. V. G. C. Sekhar, S. Chander, S. Kunjiappan and S. Murugesan, *Expert Opin. Drug Discovery*, 2021, **16**, 1119–1147.
43 A. K. Ghosh and M. Yadav, *Org. Biomol. Chem.*, 2023, **21**, 5768–5774.
44 A. K. Ghosh, M. Yadav, S. Iddum, S. Ghazi, E. K. Lendy, U. Jayashankar, S. N. Beechboard, Y. Takamatsu, S. I. Hattori, M. Amano, N. Higashi-Kuwata, H. Mitsuya and A. D. Mesecar, *Eur. J. Med. Chem.*, 2024, **267**, 116132.
45 B. J. Anson, M. E. Chapman, E. K. Lendy, S. Pshenychnyi, T. D. Richard, K. J. Satchell and A. D. Mesecar, *Res. Sq.*, 2020, DOI: 10.21203/rs.3.rs-26344/v1.
46 D. Jochmans, C. Liu and K. Donckers, *et al.*, *MBio*, 2023, **14**, e02815–e02822.
47 N. S. Zuckerman, E. Bucris, D. Keidar-Friedman, M. Amsalem and T. Brosh-Nissimov, *Clin. Infect. Dis.*, 2024, **78**, 352–355.
48 Y. Hu, E. M. Lewandowski and H. Tan, *et al.*, *ACS Cent. Sci.*, 2023, **9**, 1658–1669.
49 W. Wang, X. Zhou and W. Li, *et al.*, *Commun. Biol.*, 2025, **8**, 493.
50 Y. Zhu, I. Yurgelonis and S. Noell, *et al.*, *Sci. Adv.*, 2024, **10**, eadl4013.
51 A. J. Berkowitz, A. D. Franson, A. G. Cassals, K. A. Donald, A. J. Yu, A. K. Garimallaprabhakaran, L. A. Morrison and R. P. Murelli, *MedChemComm*, 2019, **10**, 1173–1176.
52 T. Gollnest, T. D. De Oliveira, D. Schols, J. Balzarini and C. Meier, *Nat. Commun.*, 2015, **6**, 8716.
53 A. K. Ghosh, J. Raghavaiah, D. Shahabi, M. Yadav, B. J. Anson, E. K. Lendy, S. I. Hattori, N. Higashi-Kuwata, H. Mitsuya and A. D. Mesecar, *J. Med. Chem.*, 2021, **64**, 14702–14714.
54 Z. Otwinowski and W. Minor, *Methods Enzymol.*, 1997, **276**, 307–326.
55 P. D. Adams, P. V. Afonine, G. Bunkóczi, V. B. Chen, I. W. Davis, N. Echols, J. J. Headd, L. W. Hung, G. J. Kapral, R. W. Grosse-Kunstleve, A. J. McCoy, N. W. Moriarty, R. Oeffner, R. J. Read, D. C. Richardson, J. S. Richardson, T. C. Terwilliger and P. H. Zwart, *Acta Crystallogr., Sect. D: Biol. Crystallogr.*, 2010, **66**, 213–221.
56 N. W. Moriarty, R. W. Grosse-Kunstleve and P. D. Adams, *Acta Crystallogr., Sect. D: Biol. Crystallogr.*, 2009, **65**, 1074–1080.
57 P. Emsley, B. Lohkamp, W. G. Scott and K. Cowtan, *Acta Crystallogr., Sect. D: Biol. Crystallogr.*, 2010, **66**, 486–501.
58 Please see SI data section, Table S1.